Reprinted from:

THE JOURNAL OF CHEMICAL PHYSICS VOLUME 55, NUMBER 7 1 OCTOBER 1971

Molecular Dynamics Study of Liquid Water*

ANEESUR RAHMAN

Argonne National *Laboratory, Argonne, Illinois 60439*

AND

FRANK H. STILLINGER

Bell Telephone Laboratories, Incorporated, Murray Hill, New Jersey 07974

(Received 6 May 1971)

A sample of water, consisting of 216 rigid molecules at mass density 1 gm/cm³, has been simulated by computer using the molecular dynamics technique. The system evolves in time by the laws of classical dynamics, subject to an effective pair potential that incorporates the principal structural effects of many-body interactions in real water. Both static structural properties and the kinetic behavior have been examined in considerable detail for a dynamics "run" at nominal temperature 34.3°C. In those few cases where direct comparisons with experiment can be made, agreement is moderately good; a simple energy rescaling of the potential (using the factor 1.06) however improves the closeness of agreement considerably. A sequence of stereoscopic pictures of the system's intermediate configurations reinforces conclusions inferred from the various "run" averages: (a) The liquid structure consists of a highly strained random hydrogen-bond network which bears little structural resemblance to known aqueous crystals; (b) the diffusion process proceeds continuously by cooperative interaction of neighbors, rather than through a sequence of discrete hons between positions of temporary residence. A preliminary assessment of temperature variations confirms the' ability of this dynamical model to represent liquid water realistically.

I. INTRODUCTION

Although water occupies a preeminent position among liquids, this substance has not enjoyed the attention of a rapidly developing body of statistical mechanical theory devoted specifically to its own properties.' One obvious reason for this retardation is the internal structure of the water molecule, which at the very least requires considering orientational degrees of freedom. In addition, the potentials of interaction for water molecules have until very recently[2–5] been imperfectly known. Furthermore, it now appears that these interactions are nonadditive to a significant degree.[6–9] Finally, the maximum cohesive binding between pairs of molecules, in units of k_BT at the triple point, is roughly an order of magnitude greater than the same quantity for the theoretically popular liquified noble gases.

This combination of complications renders impractical a large part of conventional liquid state theory for studying water. One must forego reliance on the integral equation approaches to static pair correlation functions on the one hand, while it is clear on the other hand that the fundamental theory of kinetic processes becomes even more complex than usual.

Under these circumstances, the most promising approach at present seems to be the direct simulation of liquid water by electronic computer. Both the "Monte Carlo" method[10] and the technique of "molecular dynamics"" are available for this purpose. The former offers the possibility of generating canonical ensembles of given temperature, but it is entirely restricted to a study of static structural properties. Molecular dynamics (which is nominally microcanonical) however can probe both static and kinetic behavior, so in -principle it is the more powerful tool. We have therefore chosen to utilize this more powerful approach. This paper provides details of computational strategy, and initial results, in our molecular dynamics investigation of liquid water.

The following Sec. II specifies the Hamiltonian used for our dynamical water model. The individual molecules are treated as rigid asymmetric rotors, i.e., their internal bond lengths and bond angles are invariant.

Classical mechanics describes the temporal evolution of our model system. The coupled differential equations for translational and rotational motion are considered in Sec. III for the model water system. Special choices are introduced there for system size (216 molecules), boundary conditions (periodic unit cell corresponding to liquid at 1 gm/cm³), and time increment for numerical integration of the coupled dynamical equations ($\Delta t = 4.355 \times 10^{-16}$ sec). Discussed as well in Sec. III is a force truncation scheme.

Section IV presents a body of results thus far accumulated which specifically bears on the static molecular structure for our water model. Separate radial correlation functions are reported for the three distinct types of nuclear pairs present (O-O, O-H, and H-H), and these are used to synthesize the hypothetical x-ray scattering pattern for the model liquid. Several aspects of the elaborate local orientational order are presented in Sec. IV by examining dipole direction correlation in successive concentric shells about a given molecule and by analyzing the oxygen–oxygen pairs in separate icosahedral sectors about a fixed molecule. The character of hydrogen bonding in the liquid has also been examined using the distribution function for pair interaction energy.

Having thus described the main features of equilibrium molecular order, we pass on to kinetic properties of the water model in Sec. V. Several autocorrelation functions are presented which reveal distinctive characteristics of translational and rotational motion. These autocorrelation functions permit one in principle to calculate the self-diffusion constant, the dielectric relaxation spectrum, neutron inelastic scattering, and NMR spin-lattice relaxation.

In order to supplement these conventional molecular dynamics quantities, we have also produced stereoscopic photographs (of a cathode-ray display) which visually present instantaneous configurations of the 216 molecules during the system's temporal evolution. Unfortunately, a printed paper such as this one does not provide an effective direct way to communicate these elaborate stereoscopic pictures. However, we have attempted verbally to summarize their contribution to our own understanding of liquid water at the appropriate points in Secs. IV and V. In particular, these pictures allow one to perceive the global features of liquid water hydrogen-bond patterns, and to appreciate details of local cooperativity in molecular Brownian motion.

The results in Secs. IV and V refer to a single computer "run" corresponding to water at a fixed temperature. Some early results for a substantially lower temperature are mentioned in Sec. VI. Although we reserve most of the details concerning temperature variations for a later publication, these few observations strengthen our conviction that the model used is a relatively faithful representation of real water.

Several items are taken up for discussion in the final Sec. VII. We list there some estensions of the present project that appear to us to have relatively high scientific merit. Included among these are possible modifications of the Hamiltonian that could well be required at the nest precision level of computer simulation for aqueous fluids. In particular, we stress a simple energy rescaling that may be applied to the present results, which seems to produce substantial improvement in agreement with experiment.

II. WATER MODEL HAMILTONIAN

Neutron diffraction studies on heavy ice[12] have confirmed earlier reasoning by Bernal and Fowler[13] and by Pauling[14] that water molecules maintain their identity in condensed phases with very little distortion of their molecular geometry. In other words, the forces of interaction between neighbors tend to be largely ineffective in perturbing the stiff covalent bonds within the molecules. From our point of view this offers the distinct advantage that the water molecules may be treated as rigid asymmetric rotors (six degrees of mechanical freedom), rather than explicit triads of nuclei (nine degrees of freedom).

The classical Hamiltonian H_N for a collection of N rigid-rotor molecules consists of kinetic energy for translational and rotational motions, plus interaction potential energy V_N:

$$H_N=\tfrac{1}{2}\sum_{j=1}^{N}(m\,|\,\mathbf{v}_j\,|^2+\boldsymbol{\omega}_j\cdot\mathbf{I}_j\cdot\boldsymbol{\omega}_j)+V_N(\mathbf{x}_1\cdots\mathbf{x}_N). \quad (2.1)$$

The molecules all have mass m. Their linear and angular velocities are, respectively, denoted by $\mathbf{v}_j$ and $\boldsymbol{\omega}_j$, while the inertial moment tensors (whose elements depend on the molecular orientation) are symbolized by $\mathbf{I}_j$. The configurational vectors $\mathbf{x}_1\cdots\mathbf{x}_N$ for the rigid molecules each comprise six components: three specify the center-of-mass position and three Euler angles fix the spatial orientation about the center of mass.

The potential energy function for any substance may always be resolved systematically into pair, triplet, quadruplet, $\cdots$, contributions[15]:

$$V_N(\mathbf{x}_1\cdots\mathbf{x}_N)=\sum_{i<j=1}^{N}V^{(2)}(\mathbf{x}_i,\ \mathbf{x}_j)+\sum_{i<j<k=1}^{N}V^{(3)}(\mathbf{x}_i,\mathbf{x}_j,\mathbf{x}_k)$$
$$+\sum_{i<j<k<l=1}^{N}V^{(4)}(\mathbf{x}_i,\ \mathbf{x}_j,\ \mathbf{x}_k,\ \mathbf{x}_l)+\cdots+V^{(N)}(\mathbf{x}_1\cdots\mathbf{x}_N). \quad (2.2)$$

The component subset functions $V^{(n)}$ occurring here have unique definitions that are generated by successive reversion of expressions (2.2) for two, three, four, $\cdots$, molecules:

$$V^{(2)}(\mathbf{x}_i,\mathbf{x}_j)\equiv V_2(\mathbf{x}_i,\ \mathbf{x}_j),$$
$$V^{(3)}(\mathbf{x}_i,\mathbf{x}_j,\mathbf{x}_k)=V_3(\mathbf{x}_i,\mathbf{x}_j,\mathbf{x}_k)-V^{(2)}(\mathbf{x}_i,\ \mathbf{x}_j)-V^{(2)}(\mathbf{x}_i,\mathbf{x}_k)-V^{(2)}(\mathbf{x}_j,\ \mathbf{x}_k),$$
$$V^{(n)}(i_1\cdots i_n)=V_n(i_1\cdots i_n)-\sum_{m=2}^{n-1}\sum_{j_1<\cdots<j_m=1}^{n}V^{(m)}(j_1\cdots j_m). \quad (2.3)$$

In the case of fluids which consist of simple nonpolar particles, such as liquid argon, it is widely believed that V_N is nearly pairwise additive. In other words, the functions $V^{(n)}$ for $n>2$ are small and hence exert insignificant influence on the local structure of the fluid. We have already noted though that water fails to conform to this sort of simplification in the strict sense. Local structure in liquid water and its solutions thus depends to a significant degree on the character of at least the three-body terms $V^{(3)}$ in Eq. (2.3), if not those of even higher order.

While it is thus unrealistic to terminate the exact water V_N after the pair terms in Eq. (2.3), it is still legitimate to employ the format of a pairwise additive potential, provided one understands that the pair functions are *effective* pair potentials, $V_{\mathrm{eff}}^{(2)}(\mathbf{x}_i,\mathbf{x}_j)$. A variational criterion is available[16] which optimally

assigns a sum of effective pair potentials to any given function $V_N(\mathbf{x}_1 \cdots \mathbf{x}_N)$; the assignment causes $V_{\text{eff}}^{(2)}$ to differ from $V^{(2)}$ in such a way that it creates essentially the same structural shifts at equilibrium that would be produced by the aggregate of triplet, quadruplet, $\cdots$, terms in Eq. (2.3). Specifically $V_{\text{eff}}^{(2)}$ is to be chosen so as to minimize the nonnegative quantity[16]:

$$\int \cdots \int \left[\exp\left[-\tfrac{1}{2}\beta V_N(\mathbf{x}_1 \cdots \mathbf{x}_N)\right] - \exp\left(-\tfrac{1}{2}\beta \sum_{i<j=1}^{N} V_{\text{eff}}^{(2)}(\mathbf{x}_i, \mathbf{x}_j)\right)\right]^2 \times d\mathbf{x}_1 \cdots d\mathbf{x}_N, \qquad \beta = (k_B T)^{-1}. \quad (2.4)$$

Our molecular dynamics calculations have been based upon a specific estimate for the liquid water $V_{\text{eff}}^{(2)}$ that has been proposed by Ben-Naim and Stillinger.[17] This estimate consists of a part v_{LJ} depending only on oxygen-oxygen separation r_{ij}, plus a function v_{el} [modulated by a factor $S(r_{ij})$] that sensitively depends upon orientations about the oxygen nuclei:

$$V_{\text{eff}}^{(2)}(\mathbf{x}_i, \mathbf{x}_j) = v_{\text{LJ}}(r_{ij}) + S(r_{ij}) v_{\text{el}}(\mathbf{x}_i, \mathbf{x}_j). \quad (2.5)$$

The quantity v_{LJ} is a potential of the Lennard-Jones (12-6) type:

$$v_{\text{LJ}}(r_{ij}) = 4\epsilon[(\sigma/r_{ij})^{12} - (\sigma/r_{ij})^{6}]. \quad (2.6)$$

Since the water molecule and the neon atom are isoelectronic closed-shell systems, parameters ϵ and σ in Eq. (2.6) were chosen by Ben-Naim and Stillinger to be the accepted neon values[18]:

$$\epsilon = 5.01 \times 10^{-15} \text{ erg} = 7.21 \times 10^{-2} \text{ kcal/mole}, \qquad \sigma = 2.82 \text{ Å}. \quad (2.7)$$

Four point charges, each exactly 1 Å from the oxygen nucleus, are imagined to be embedded in each water molecule in order to produce v_{el}. These charges are arranged to form the vertices of a regular tetrahedron. Two of them are positive ($+0.19e$ each) to simulate partially shielded protons, while the remaining two ($-0.19e$ each) act roughly as unshared electron pairs. The set of 16 charge pair interactions between two molecules forms v_{el}:

$$v_{\text{el}}(\mathbf{x}_i, \mathbf{x}_j) = (0.19e)^2 \sum_{\alpha_i, \alpha_j = 1}^{4} (-1)^{\alpha_i + \alpha_j} / d_{\alpha_i \alpha_j}(\mathbf{x}_i, \mathbf{x}_j). \quad (2.8)$$

Here the indices α_i and α_j are even for positive charges, odd for negative charges. The distance $d_{\alpha_i \alpha_j}$ between the subscripted charges obviously depends on the full set of relative configurational variables for molecules i and j.

If the radial distance r_{ij} between oxygen nuclei were 2 Å or less, it would be possible for one of the distances $d_{\alpha_i \alpha_j}$ to be zero. The resultant divergence of v_{el} surely would be physically meaningless. The "switching function" $S(r_{ij})$ however suppresses this possibility by vanishing identically at these small separations. In fact S varies continuously and differentially between 0 (small r_{ij}) and 1 (large r_{ij}):

$$S(r_{ij}) = 0 \qquad (0 \le r_{ij} \le R_L),$$
$$= (r_{ij} - R_L)^2 (3R_U - R_L - 2r_{ij})/(R_U - R_L)^3 \qquad (R_L \le r_{ij} \le R_U),$$
$$= 1 \qquad (R_U \le r_{ij} < \infty), \quad (2.9)$$

where[17]

$$R_L = 2.0379 \text{ Å}, \qquad R_U = 3.1877 \text{ Å}. \quad (2.10)$$

The effective pair potential (2.5) incorporates the tendency of water molecules to associate by hydrogen bonding. The absolute minimum of $V_{\text{eff}}^{(2)}(\mathbf{x}_i, \mathbf{x}_j)$ is achieved when one molecule forms a linear H bond (of length $r_{ij} = 2.76$ Å) to the rear of the other molecule, i.e., when a charge $+0.19e$ on one is lined up with (but 0.76 Å distant from) a charge $-0.19e$ on the other. In this minimum energy configuration, the fully formed H bond has energy[17]

$$V_{\text{eff}}^{(2)}(\mathbf{x}_i, \mathbf{x}_j)|_{\min} = -4.514 \times 10^{-13} \text{ erg} = -6.50 \text{ kcal/mole pairs}. \quad (2.11)$$

Figure 1 illustrates this pair configuration, which after identification of its positive charges as proton positions agrees rather well with the stable dimer geometry predicted by *ab initio* quantum mechanical calculations.[6-9]

The distribution of mass in each molecule follows the tetrahedral geometry utilized in $V_{\text{eff}}^{(2)}$. The oxygen atom mass ($2.65.5.5 \times 10^{-23}$ g) is concentrated at the center of the tetrahedron (the force center for v_{LJ}). A mass equal to $\frac{1}{16}$ this value is placed at each of the two positions bearing charges $+0.19e$ that are 1 Å away from the tetrahedron center, to act as

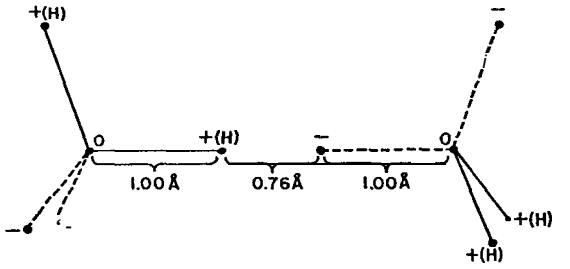

FIG. 1. Minimum energy configuration for two water molecules, according to potential (2.5). Each oxygen nucleus is symmetrically surrounded by a tetrad of four-point charges ($\pm 0.19e$), the positive members of which represent partially shielded protons. The configuration shown has a plane of symmetry and incorporates a single linear H bond.

hydrogen atom masses.[19] The center of mass is therefore displaced along the molecular symmetry axis by 0.06415 Å, away from the oxygen mass. This rigid mass distribution of course fixes the inertial moment tensor for each molecule.

Investigation of the structure of ice crystals and the clathrate hydrates is not our primary objective in this paper. But the tetrahedral charge arrangements which underlie $V_{\rm eff}^{(2)}$ strongly favor the local tetrahedral pattern of H bonds about each molecule observed in these aqueous solids. Therefore there can be little doubt that $V_{\rm eff}^{(2)}$ in Eq. (2.8) will permit the existence of mechanically stable H-bond networks filling space in the ice and clathrate patterns. Our task now is to employ the effective pair potential version of the Hamiltonian:

$$H_N=\tfrac{1}{2}\sum_{j=1}^{N}(m\ (\mathbf{v}j\ |^2+\boldsymbol{\omega}_j\cdot\mathbf{I}_j\cdot\boldsymbol{\omega}_j)+\sum_{i<j=1}^{N}V_{\rm eff}^{(2)}(\mathbf{x}_i,\ \mathbf{x}j) \tag{2.12}$$

under liquid-phase conditions, to see what type of nonperiodic, strained, and defective H-bond networks spontaneously appear.

III. DYNAMICAL EQUATIONS AND METHOD OF SOLUTION

The configurational vector $\mathbf{x}_j$ for molecule j involves the following components:

$$\mathbf{x}_j=(X_j, Y_j, Z_j, \alpha_j, \beta_j, \gamma_j)\,. \tag{3.1}$$

The first three are the Cartesian coordinates of the molecule's center of mass. The Euler angles α_j, β_j, and γ_j specify the orientation of the molecule's principal axes relative to a standard laboratory fixed orientation in the manner shown by Fig. 2. These angles have the following limits:

$$0\leq\alpha, \gamma<2\pi, \qquad 0\leq\beta\leq\pi. \tag{3.2}$$

The dynamical equations required to describe the temporal evolution of a set of rigid-rotor molecules are the coupled Newton-Euler equations. In the case of the center-of-mass position $\mathbf{R}_j=$ **(Xj,** Y_j, **Zj)** for molecule j we have

$$\text{wz}\ (d^2\mathbf{R}_j/dt^2)=\mathbf{F}_j, \tag{3.3}$$

where $\mathbf{F}_j$ is the total force exerted on that molecule by all others:

$$\mathbf{F}_j=-\nabla_{R_j}\sum_{k(\neq j)}V_{\rm eff}^{(2)}\ (\mathbf{xj},\ \mathbf{x}_k)\,. \tag{3.4}$$

In an analogous fashion, rotational motion involves the torque $\mathbf{N}_j$ exerted on molecule j. The inertial moment tensor $\mathbf{I}_j$ is diagonal (I_1, I_2, I_3) in a Cartesian coordinate system affixed to the molecule as shown in Fig. 2. If we denote this molecule fixed

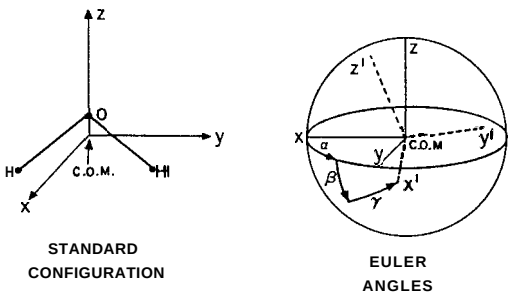

FIG. 2. Euler angle definition for waler molecule orientation. The "standard configuration" relative to laboratory fixed coordinate system has $\alpha=\beta=\gamma=0$; the molecule lies in the yz plane, and z is the twofold molecular axis. The arcs denoted by α, β, and γ on the sphere surface are the path described by the molecule fixed axis x'. α is an angle of rotation about the initial $z=z'$ axis, β gives a rotation about the resulting y' axis, and finally, γ is a rotation angle about the displaced z' axis.

system by primes, then the corresponding torque components are

$$\mathbf{N}_j=(N_{jx'}, N_{jy'}, N_{jz'})\,. \tag{3.5}$$

In the same coordinate system, the angular velocity components must obey the Euler equations[20]:

$$\begin{aligned}
&I_1(d\omega_{jx'}/dt)-\omega_{jy'}\omega_{jz'}(I_2-I_3)=N_{jx'},\\
&I_2(d\omega_{jy'}/dt)-\omega_{jz'}\omega_{jx'}(I_3-I_1)=N_{jy'},\\
&I_3(d\omega_{jz'}/dt)-\omega_{jx'}\omega_{jy'}(I_1-I_2)=N_{jz'}.
\end{aligned} \tag{3.6}$$

The angular velocity components have the following representation in terms of the Euler angles of Fig. 2[21]:

$$\begin{aligned}
\omega_{jx'}&=(d\alpha_j/dt)\sin\beta_j\sin\gamma_j+(d\beta_j/dt)\cos\gamma_j,\\
\omega_{jy'}&=(d\alpha_j/dt)\sin\beta_j\cos\gamma_j-(d\beta_j/dt)\sin\gamma_j,\\
\omega_{jz'}&=(d\alpha_j/dt)\cos\beta_j+(d\gamma_j/dt)\,.
\end{aligned} \tag{3.7}$$

From the computational point of view, it is convenient to cast the dynamical equations into dimensionless form. The parameters ϵ and σ, Eqs. (2.7), serve as units for energy and length. Then by invoking the total molecular mass m, the natural time unit becomes $\sigma(m/\epsilon)^{1/2}$; for water this is 2.179×10^{-12} sec.

Our calculations involve $N=216$ water molecules placed in a cubical container and subject to periodic boundary conditions so as to eliminate undesirable wall effects. This assembly is maintained at mass density 1 g/cm³ by fixing the cube side at $6.604\sigma=18.62$ Å. The corresponding number density ρ is 3.344×10^{22}/cm³.

Under periodic boundary conditions, each molecule would interact with an infinite number of others, including the remaining 215 in the same unit cell as well as all periodic images filling the entire space. In principle, then, Ewald sums would have to be carried out to evaluate the potential energy. In order

to facilitate the molecular dynamics calculation,[22] it is advisable instead to include interactions only up to some finite limiting distance. In the present work, each molecule's oxygen nucleus is regarded as residing at the center of a sphere with radius 3.25σ, and only those other molecules having oxygens within this sphere are considered in computing the force and torque on the central molecule. By experimentation with various cutoff radii, it seems that the choice of cutoff at 3.25σ probably commits little error in predicted liquid structure, relative to a full Ewald sum (infinite cutoff radius). As with the full Ewald sum, the truncated dynamical equations maintain the initial periodicity at all times.

In the case of a substance such as Ar, with spherically symmetric particles, a force cutoff in the Newtonian equations of motion does not affect the role of energy as a constant of the motion, i.e., the system remains conservative. However with noncentral interactions as water requires, a truncation of force and torque terms in the coupled Newton-Euler equations leads in principle to a nonconservative situation.[23] Over a long dynamical run, this irreversibility would lead to a secular rise in temperature, as though the system were weakly coupled to a high-temperature heat reservoir. We have found, however, that this effect is manageable for the runs involved in the present investigation.

The calculations were carried out at the Argonne National Laboratory on an IBM 360-50-75 computer.[24] Details of the algorithm utilized to integrate the differential equations of motion are contained in Appendix A. By experimenting with two-molecule dynamics, an appropriate choice for the basic time increment for the numerical integration was found to be the following:

$$\Delta t = 2\times 10^{-4}\times\sigma(m/\epsilon)^{1/2} = 4.353\times 10^{-16}\ \text{sec}. \tag{3.8}$$

The smallness of this increment (relative to that required in liquid Ar calculations[22]) stems from the rapid angular velocity of the water molecules, which in turn derives from the small mass of the protons. To advance the system by At, the computer requires about 40 sec, so a time dilation factor of about 10^{17} applies in the relationship of real water molecule motions to those in our computation.

The 216 molecules were placed initially within the periodic cell at arbitrary positions, with random orientations, and with no translational or rotational velocities. Since this configuration corresponded to a very large potential energy, the velocities quickly increased to a distribution characteristic of about $2\times 10^4\ ^\circ\text{K}$ within a few *At* steps. The system was then interrupted, and all velocities set to zero at the momentary configuration that obtained. This served to remove some of the excess energy. After several more At steps, the molecules again had achieved high velocities, so once again they were set equal to zero. Several repetitions of this energy reduction procedure were required to bring the ambient temperature near to the desired range. Thereafter, fractional uniform adjustment of all velocities permitted fine temperature control. In all, over 5000 steps of length At were expended in achieving the proper system energy and in allowing the system to "age." After this interval, the subsequent period of 5000 At was actually the time interval over which the molecular dynamics statistical averages reported below were calculated. We believe that the system had developed in time long enough to eliminate any undesirable remanent effects due to the choice of initial conditions.

Temperature is inferred from the average values of the translational and rotational kinetic energies over the molecular dynamics run; in a sufficiently long run:

$$\langle \tfrac{1}{2}\sum_{j=1}^{N} m\,|\,\mathbf{v}_j\,|^2\rangle = \langle \tfrac{1}{2}\sum_{j=1}^{N} \boldsymbol{\omega}_j\cdot\mathbf{I}_j\cdot\boldsymbol{\omega}_j\rangle = \tfrac{3}{2}Nk_BT. \tag{3.9}$$

Temperature variations for a new calculation can be implemented by suitably modifying linear and angular momenta at the end of a previous run, provided the system is allowed to "age" appropriately.

Integrating the dynamical equations in dimensionless form has the advantage that if length or strength rescaling of the potential ultimately proves to be required, results may be trivially renormalized to accommodate those changes. Thus if $V_{\text{eff}}^{(2)}$ were to be multiplied by the scalar factor $1+\zeta$, the energy unit would become $(1+\zeta)\epsilon$, and the unit of time would change to $\sigma[m/(1+\zeta)\epsilon]^{1/2}$. In view of Eq. (3.9), this would require that the temperature T originally assigned to a given molecular dynamics run be reinterpreted as $(1+\zeta)T$.

IV. STATIC STRUCTURE

From the average kinetic energy calculated for the 5000 step molecular dynamics run, the temperature of the system was determined to be 307.5°K (34.3°C). The force-torque cutoff irreversibility actually caused the total energy to drift upward by 1.5% during the run, with a mean value per molecule:

$$\langle H_N\rangle/N = -101.85\,\epsilon; \tag{4.1}$$

the potential energy contribution to this total was

$$\langle V_N\rangle/N = -127.3\,\epsilon = -9.184\ \text{kcal/mole}. \tag{4.2}$$

(The experimental value of this last quantity at 34.3°C is -9.84 kcal/mole.) Though the temperature effectively drifted upward during the computation,

the structural features to be reported as run averages should correspond to the computed mean temperature 34.3°C for the run.

A. Radial Pair Correlation Functions

In water the three distinct types of nuclear pairs lead to three corresponding radial pair correlation functions, $g_{OO}^{(2)}(r)$, $g_{OH}^{(2)}(r)$, and $g_{HH}^{(2)}(r)$. These are defined for present purposes by the requirement that

$$\rho_\alpha \rho_\beta g_{\alpha\beta}^{(2)}(r)\, dv_1 dv_2 \qquad (\alpha, \beta = O, H) \tag{4.3}$$

equal the fraction of time that differential volume elements dv_1 and dv_2 (separated by distance r) simultaneously and respectively contain nuclei of species α and β from distinct molecules. Here ρ_α and ρ_β stand for the number densities of the nuclei. In the large system limit, these radial pair correlation functions for a fluid phase all approach unity as $r \to \infty$.

Figure 3 exhibits the computed $g_{OO}^{(2)}(r)$, out to distance 3.25σ (9.165 Å), along with the "running coordination number":

$$n_{OO}(r) = 4\pi\rho_O \int_0^r s^2 g_{OO}^{(2)}(s)\, ds. \tag{4.4}$$

The important features of the $g_{OO}^{(2)}(r)$ curve to note are the following:

(a) The relatively narrow first peak, with maximum at $r/\sigma = 0.975$, comprises an average of 5.5 neighbors out to the following minimum at $r/\sigma = 1.22$.

(b) The second peak is low and broad, with a maximum at about $r/\sigma = 1.65$. The ratio of second-peak to first-peak distances (1.69) is close to that observed for the ideal ice structure ($2\sqrt{2}/\sqrt{3} = 1.633$), where successive neighbor hydrogen bonds occur at the tetrahedral angle 109°28′.

(c) There is substantial filling between the first and second peaks.

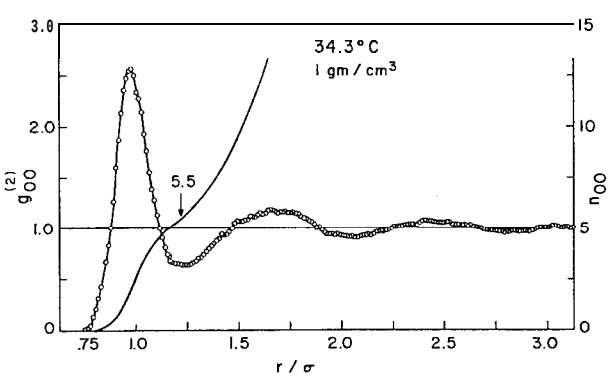

FIG. 3. Oxygen nucleus pair correlation function $g_{OO}^{(2)}$. The monotonically rising curve n_{OO} shows the average number of neighbor oxygens within any radial distance r. The liquid has temperature 34.3°C and density 1 g/cm³.

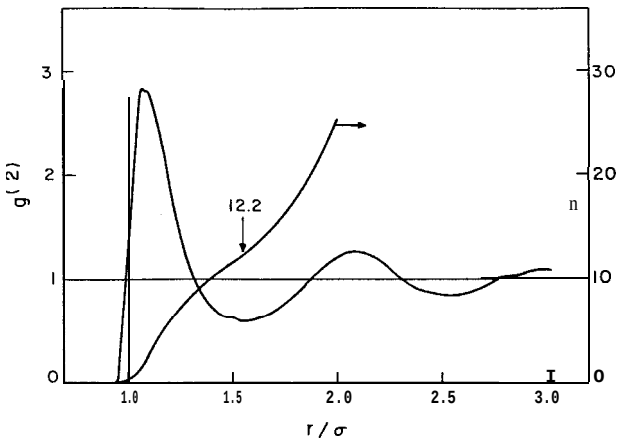

FIG. 4. Pair correlation function for liquid Ar. The reduced state parameters are $\rho^* = \rho\sigma^3 = 0.81$ and $T^* = k_B T/\epsilon = 0.74$. $n(r)$ gives the running neighbor count (right-hand scale).

(d) Although a weak third peak appears at $r/\sigma \cong 2.45$, the $g_{OO}^{(2)}$ curve has begun to damp rapidly to its asymptotic value unity. Beyond $r/\sigma = 3.00$ (8.46 Å), deviations from unity are apparently insignificant.

This liquid water pair correlation function stands in distinct contrast to its analog in liquid Ar, for which it is traditional to assume that the pair potential involves *only* a central Lennard-Jones interaction, and no directional forces. Figure 4 presents a liquid Ar $g^{(2)}(r)$, specially computed by the molecular dynamics procedure of Ref. 22, for comparison. Not only does the first peak encompass more neighbors than water (12.2 with a cutoff at the first minimum), but the distance ratio of second and first peaks (1.90) is considerably larger.

Evidently there is a substantial difference in the type of disordering attendant upon melting ice to liquid water on the one hand, and melting a face-centered cubic crystal of Ar to the corresponding liquid Ar on the other hand. The ice lattice second-neighbor peak, although broadened considerably, clearly remains after melting. The same is not the case for Ar, however, since Fig. 4 shows no persistence of the fcc lattice second-neighbor distance at $2^{1/2}$ times the first neighbor distance. Obviously the directionality of interactions in liquid water exerts a profound influence, not present in other liquids, on local order.

Figures 5 and 6, respectively, show $g_{OH}^{(2)}$ and $g_{HH}^{(2)}$ for water (these of course have no analogs in liquid Ar). The former of these functions plays a role in the theory of solute structural shifts in aqueous solutions.% The prominent first two peaks displayed by $g_{OH}^{(2)}$ evidently arise from neighboring molecules that are hydrogen bonded; the peak at smaller separation involves the proton along the bond and the acceptor oxygen toward which it points, while the larger dis-

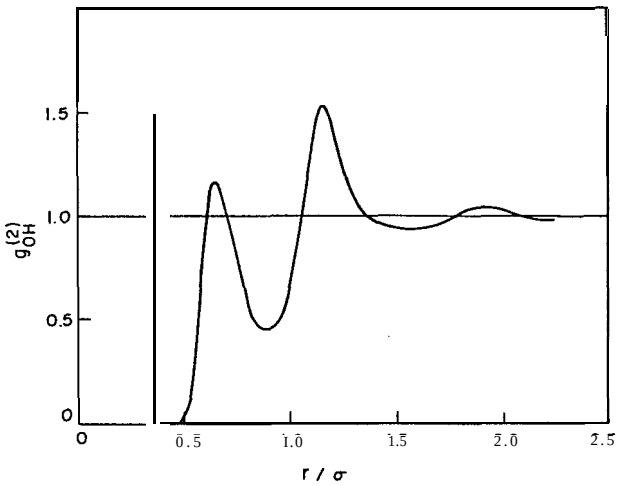

FIG. 5. Cross correlation function $g_{OH}^{(2)}(r)$ for water; 34.3°C and 1 g/cm³. The vertical line indicates the intramolecular O-H covalent bond length.

tance second peak comprises all remaining oxygen–proton distances across the bonded pair of molecules. The interpretation of $g_{HH}^{(2)}$ is less direct, owing to the multiplicity of possible proton pairs in hydrogen-bond networks, but it seems safe to assign the first peak to a proton along a hydrogen bond and a proton in the acceptor molecule. The very distinct shoulder in $g_{HH}^{(2)}$ in the region $r/\sigma \approx 0.5$ is especially interesting, since these very close proton pairs may in part arise from the situation in which three proton donors crowd together at the negative rear of an acceptor molecule.

Even in the absence of further information, the three water correlation functions lead to a picture of liquid water as a random, defective, and highly strained network of hydrogen bonds that fills space rather uniformly. The fact that each of the three correlation functions approaches its asymptotic value unity rather quickly as r increases indicates that large, low density clusters or "icebergs" are not present to a significant degree, though they have occasionally been advocated to explain the properties of water.[26,27] Recent small angle x-ray scattering measurements on liquid water appear to be consistent with this observation.[28]

Unfortunately, experiments have not been carried out to provide measurements of the separate functions $g_{OO}^{(2)}, g_{OH}^{(2)}$, and $g_{HH}^{(2)}$ for direct comparison with the molecular dynamics results. In principle this could be done by combining x-ray scattering results with neutron scattering intensities for isotopically substituted waters. At present, though, only x-ray scattering has been carried out, which provides a weighted average of the three pair correlation functions.[29] We have therefore utilized our separate correlation functions, along with tabulated atomic scattering factors,[29] to synthesize the x-ray scattering intensity $I(s)$ [$s = (4\pi/\lambda)\sin\theta$, the magnitude of the scattering vector].

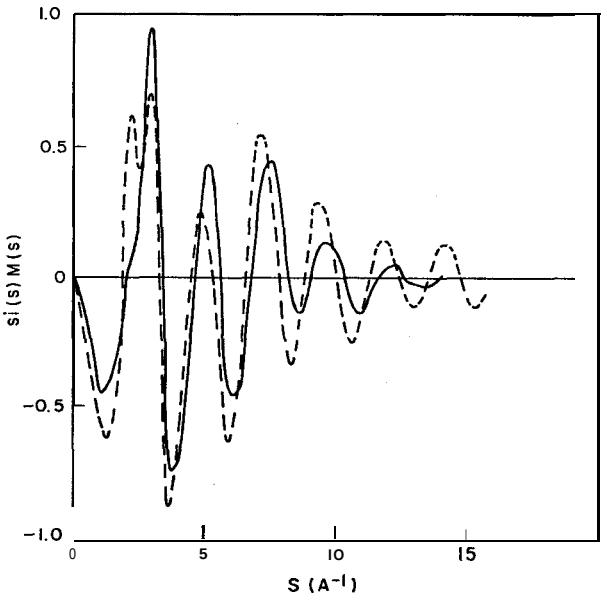

FIG. 7. Theoretical (solid line), and experimental (dotted line), x-ray scattering intensities for liquid water. The latter are taken from Narten, Ref. 29, and refer to 25°C.

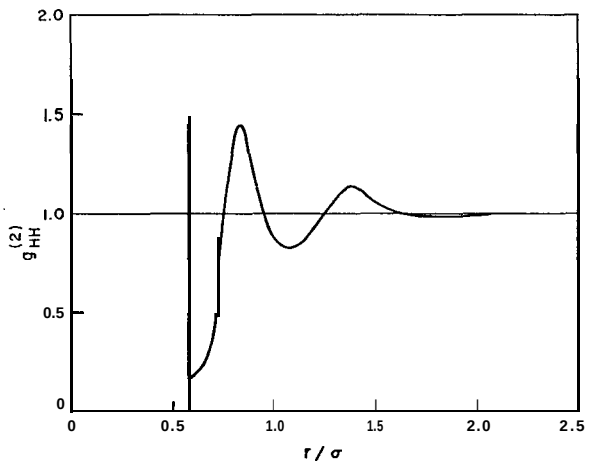

FIG. 6. Proton pair correlation function $g_{HH}^{(2)}(r)$ for water; 34.3°C and 1 g/cm³. The vertical line indicates the intramolecular H-H pair distance.

Figure 7 presents computed values of $sI(s)$, along with Narten, Danford, and Levy's measurements of the same quantity at their nearest temperature, 25°C.[29] Agreement obtains only in modest degree, with the principal discrepancy occurring at the first peak ($s \approx 1.7$ to 3.0 Å^{-1}). At present it is not clear that the disagreement arises entirely from shortcomings in

our basic water model. It may be, for example, that covalent intramolecular chemical bonds, and intermolecular hydrogen bonds, distort electron distributions sufficiently to invalidate the conventional assumption of independent spherically symmetric atomic scattering factors. In addition, we have treated the intramolecular geometry of nuclear positions as rigid, whereas the substantial zero-point motions should actually be taken into account to predict I(s). More work is clearly required in this area, beyond the scope of the present paper.

B. Icosahedral $g_{OO}^{(2)}$ Resolution

The radial pair correlation function $g_{OO}^{(2)}(r)$ gives the mean density of oxygen nuclei over concentric spherical shells about a fixed oxygen nucleus. It thus provides little information about the angular distribution of oxygens on those shells if the molecule to which the central one belongs is held fixed in orientation. This angular information is important, however, if one is to understand the detailed architecture of hydrogen bond networks in liquid water.

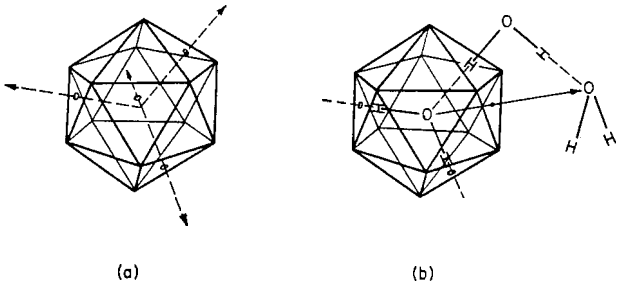

FIG. 8. Geometric basis of the icosahedral $g_{OO}^{(2)}$ resolution. In (a), a tetrahedrally directed quartet of directions passes simultaneously through the centroids (open circles) of four faces of a regular icosahedron. The correspondingly oriented water molecule is shown in (b). The four pierced faces in (a) form class I, the 12 faces sharing an edge with these four form class II, and the remaining four faces form class III.

The basic tetrahedral symmetry of our model water molecules suggests a convenient way to resolve some of the angular detail. Figure 8(a) shows that the four tetrahedral directions emanating from a point can be made to pass simultaneously through the centroids of four noncontiguous triangular faces of a regular icosahedron centered at that point, The four tetrahedral vectors in fact are perpendicular to the faces that they pierce. In Fig. 8(b), accordingly, a water molecule has been placed with its oxygen nucleus at the icosahedron center, and has been oriented so that the directions of the four undistorted hydrogen bonds in which it can engage pass through face centroids.

Let us denote the pierced triangular faces by I. Then first neighbors of a given water molecule which interact via undistorted hydrogen bonds with that molecule (as in ice) will invariably have their oxygen nuclei within those solid angles about the icosahedron center which are generated by class I faces.

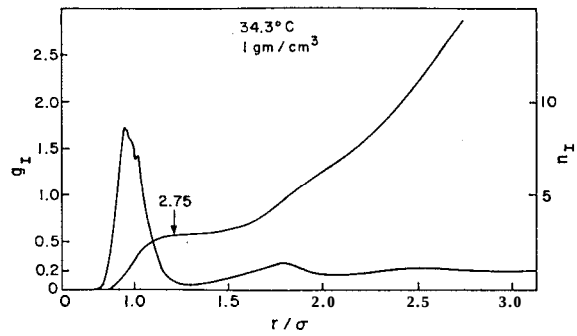

FIG. 9. $g_I(r)$ and $n_I(r)$ for water at 34.3°C and 1 g/cm³.

Twelve more icosahedron faces share edges with the four of class I. This new class of faces will be called class II. It is clear from Fig. 8(b) that second neighbor oxygens, located along a sequence of two undistorted hydrogen bonds, will occur within solid angles generated only by class II faces. Rotation around linear hydrogen bonds can cause the second-neighbor oxygen-oxygen direction to move across class II faces in an arc, but this arc will pass from one II face to another II face through a shared vertex.

The four I faces and twelve II faces leave four other faces to be accounted for. These are the "anti-tetrahedral faces," which lie directly opposite those of class I, across the icosahedron. We shall denote them by III. In a network of undistorted hydrogen bonds, oxygen nuclei from third- or higher-order neighbors only can occur in solid angles generated by class III faces.

The fact that the full solid angle 4π about the central oxygen in Figs. 8 has been split into three parts, I, II, and III, means that a corresponding resolution of $g_{OO}^{(2)}$ can be effected:

$$g_{OO}^{(2)}(r) = g_I(r) + g_{II}(r) + g_{III}(r), \qquad (4.5)$$

where the three functions with Roman numeral sub-

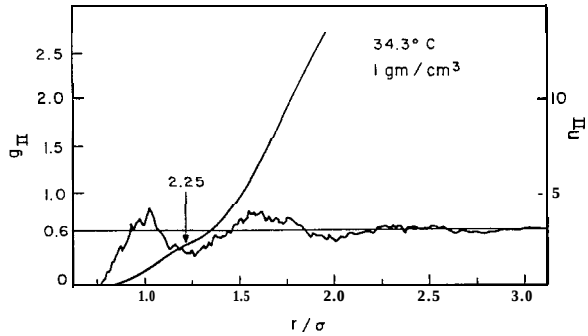

FIG. 10. $g_{II}(r)$ and $n_{II}(r)$ for water at 34.3°C and 1 g/cm³.

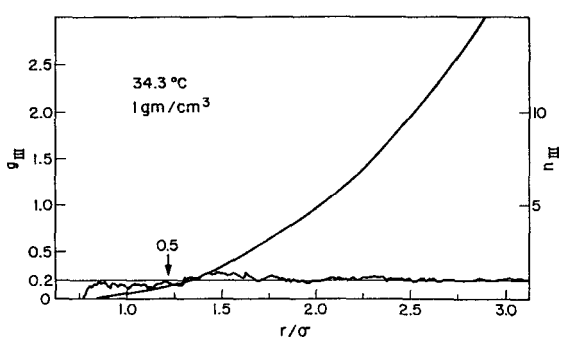

FIG. 11. $g_{III}(r)$ and $n_{III}(r)$ for water at 34.3°C and 1 g/cm³.

scripts represent the relative occurrence probabilities, at radial distance r, of oxygen nuclei in the respective solid angle classes. We will have

$$\lim_{r\to\infty} g_{I}(r) = \lim_{r\to\infty} g_{III}(r) = \tfrac{1}{5},$$
$$\lim_{r\to\infty} g_{II}(r) = \tfrac{3}{5}, \tag{4.6}$$

reflecting merely the fraction of all 20 icosahedral faces in the respective classes.

Figures 9-l 1, respectively, present our computed functions g_I, g_{II}, and g_{III} for 34.3°C. Shown as well in each of these Figures are the corresponding running coordination numbers, defined in analogy to Eq. (4.4), e.g.,

$$n_I(r) = 4\pi\rho_0 \int_0^r s^2 g_I(s)\, ds. \tag{4.7}$$

These results very clearly demonstrate that substantial deviations from ideal hydrogen-bonding directions are present. Although $g_I(r)$ exhibits a large peak at the position of the first $g_{OO}^{(2)}(r)$ maximum $(r/\sigma \cong 1)$, $g_{II}(r)$ also has substantial weight there as well. Evidently some of the hydrogen bonds to neighbors have been bent out of class I solid angles into those contiguous solid angles of class II. On the basis of the curves $n_{OO}(r)$ and $n_{II}(r)$, evaluated at the first $g_{OO}^{(2)}(r)$ minimum, 2.25/5.50, or 41%, of the bonds suffer this fate. In addition, neither g_I nor g_{III} vanish at $r/\sigma = 1.633$, where ideally bonded second neighbors should appear only in g_{II}.

The function $g_{III}(r)$ shown in Fig. 11 is nearly flat from $r/\sigma = 0.75$ onward. For $r/\sigma \geq 2$ this is easy to understand merely in terms of the large number of ways that successive hydrogen bonds can link neighboring molecules so as to place ultimately an oxygen nucleus in a class III solid angle region. But when r/σ is near unity, the pairs which contribute to g_{III} are necessarily so seriously misaligned that no hope for a hydrogen bond between them exists. One possible explanation would be that an "interstitial" molecule were involved in such a pair, surrounded by, but only weakly interacting with, an enclosing network of hydrogen bonds. Alternatively, two molecules each incompletely hydrogen bonded to their surroundings, could by chance simply back into one another.

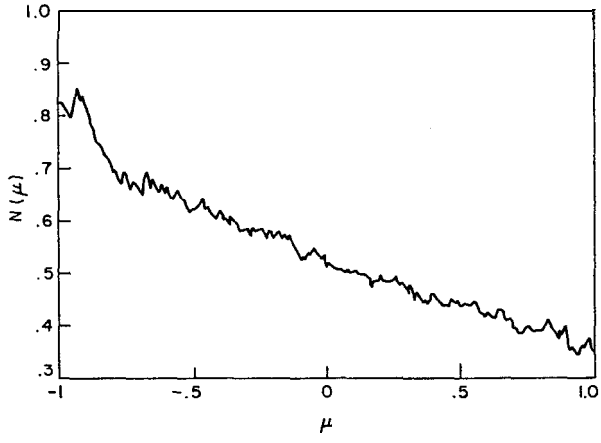

FIG. 12. Distribution function $N(\mu)$ for $\mu = \cos\theta_1$, defined by Eq. (4.13). The decline with increasing μ indicates a tendency for $\mathbf{u}_1^{(1)}$ and $\mathbf{N}_1$ to be antiparallel.

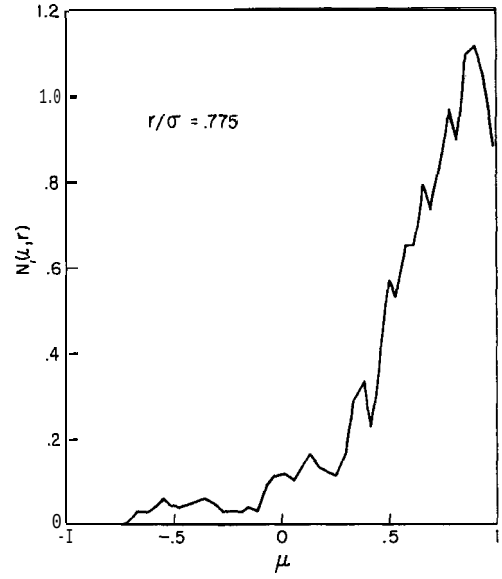

FIG. 13. Distribution function $N(\mu, r)$ for the angle cosine (μ) between a given molecule's dipole direction and the direction of the total moment of neighbors at distance r. Distances are reckoned in terms of oxygen atom positions. For this graph, $r = 0.775\sigma$.

C. Dipole Direction Correlation

The dipole moment of an undisturbed water molecule bisects its HOH bond angle. As another aspect of static orientational order in liquid water, it is interesting to see how these dipole directions are distributed for neighboring molecules.

Let $\mu_i^{(1)}$ represent a unit vector along the dipole direction of molecule i, and set M equal to their vector sum for all $N=216$ molecules:

$$\mathrm{M}=\sum_{i=1}^{N}\mu_i^{(1)}. \tag{4.8}$$

If the dipole directions were entirely uncorrelated,

$$\langle M^2\rangle/N=1 \qquad \text{(uncorrelated)}\ . \tag{4.9}$$

Instead, the average computed for the molecular dynamics run turns out to be

$$\langle M^2\rangle/N=0.171 \qquad \text{(molecular dynamics)}, \tag{4.10}$$

so evidently the molecular interactions act in a way to quench the system's net moment.

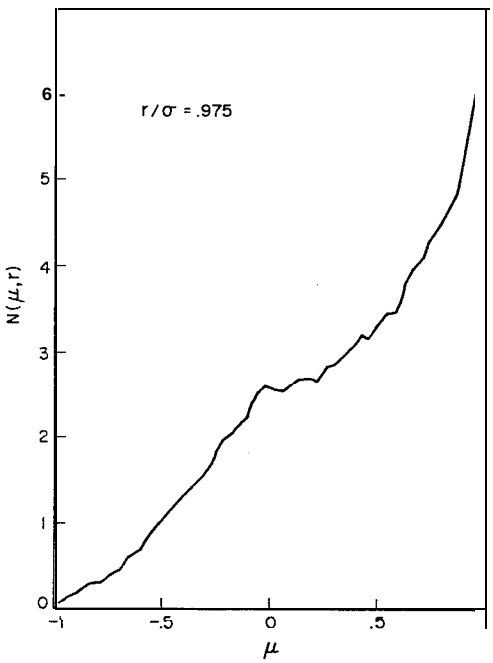

FIG. 14. Orientational distribution function $N(\mu,r)$ for $r=0.975\sigma$.

This quenching effect may be examined in a variety of alternative ways. One can, for instance, isolate one of the molecules (which for convenience we take to be the one numbered 1), and ask how its own dipole direction correlates with

$$\mathbf{N}_1=\mathbf{M}-\mu_1^{(1)}, \tag{4.11}$$

the total moment of all the other molecules. Of course the magnitude of $\mathbf{N}_1$ fluctuates, as revealed by the difference in computed averages:

$$\langle|\mathbf{N}_1|\rangle=5.69,$$
$$\langle N_1^2\rangle^{1/2}=6.13, \tag{4.12}$$

as well as its direction relative to $\mu_1^{(1)}$. The relevant

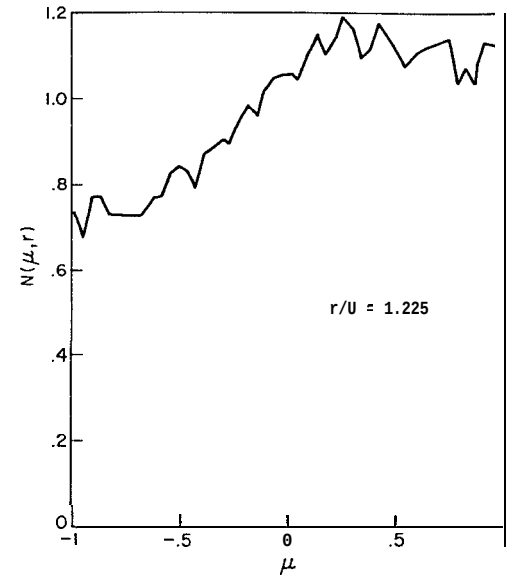

FIG. 15. Orientational distribution function $N(\mu,r)$ for $r=1.225\sigma$.

angle θ_1 is defined by

$$\cos\theta_1=\hat{\mathbf{N}}_1\cdot\mu_1^{(1)}, \qquad \hat{\mathbf{N}}_1=\mathbf{N}_1/|\,\mathbf{N}_1\,|. \tag{4.13}$$

For our molecular dynamics run:

$$\langle\cos\theta_1\rangle=-0.129, \tag{4.14}$$

showing that on the average, $\mathbf{N}_1$ and $\mu_1^{(1)}$ point in opposite directions.

Figure 12 shows the full distribution function $N(\mu)$ for $\mu=\cos\theta_1$, for which the average value shown in (4.14) applies. Although this distribution is nearly linear, a slight positive curvature beyond statistical uncertainty seems to be present.

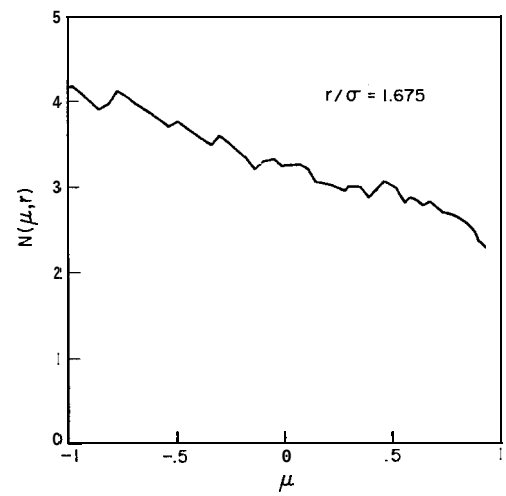

FIG. 16. Orientational distribution function $N(\mu,r)$ for $r=1.675\sigma$.

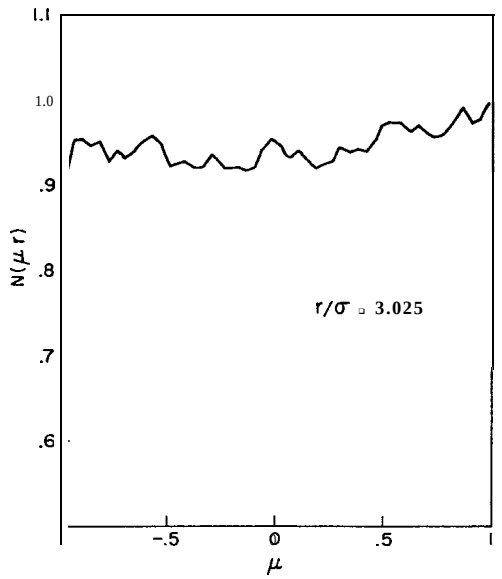

FIG. 17. Orientational distribution function $N(\mu,r)$ for $r=3.025\sigma$.

It is also instructive to analyze the separate contributions to N_1 from distinct spherical shells centered about the oxygen nucleus of molecule 1. Figures 13-17 exhibit partial distribution functions $N(\mu,r)$ for μ, the cosine of the angle between $\mu_1^{(1)}$ and the moment of a molecule contained within a shell of mean radius r, and width 0.05σ. The first two of the figures ($r/\sigma=0.755$ and 0.975, respectively) show that pairs of molecules close enough to hydrogen bond have a strong tendency toward dipole parallelism ($\mu=+1$), in spite of the over-all opposite tendency which is manifest in Fig. 12. At the somewhat larger distance $r/\sigma=1.225$ (Fig. 15), the alignment effect is less distinct, and it has reversed at $r/\sigma=1.675$ (Fig. 16). Figure 17 indicates a relatively flat distribution for $r/\sigma=3.025$.

The static dielectric constant ϵ_0 for polar fluids is intimately connected to the orientational correlations between neighboring molecules. The Kirkwood theory of polar dielectrics[30] expresses ϵ_0 in terms of the mean molecular polarizability α, the liquid phase dipole moment μ_l, and an orientational correlation function g_K:

$$(\epsilon_0-1)(2\epsilon_0+1)/3\epsilon_0=4\pi\rho[\alpha+(\mu_l^2 g_K/3k_BT)]. \quad (4.15)$$

The Rirkwood orientations1 correlation factor g_K may be expressed in terms of the full orientation and position dependent pair correlation function $g^{(2)}(\mathbf{x}_1,\mathbf{x}_2)$[17,31]:

$$g_K=1+(\rho/8\pi^2)\int d\mathbf{x}_2(\boldsymbol{\mu}_1^{(1)}\cdot\boldsymbol{\mu}_2^{(1)})g^{(2)}(\mathbf{x}_1,\ \mathrm{a}); \quad (4.16)$$

in this expression one must be careful to use only the infinite system limit function $g^{(2)}(\mathbf{x}_1,\mathbf{x}_2)$.

Our molecular dynamics calculation has not been set up in such a way that direct evaluation of ϵ_0 is possible. No external electric field is involved, of course. Furthermore, μ_l is unknown except to the extent that it should exceed the free molecule moment; even in ice, where the local structure is completely known, estimates of the mean molecular dipole moment vary considerably.[32,33]

Nevertheless, enough information is supplied by our calculation to evaluate g_K. The evaluation is not direct, however, since the infinite system limit required of $g^{(2)}$ in Eq. (4.16) is not available. Instead, only a finite system $g^{(2)}$ is at hand, and its finite limit integral analog of (4.16) gives an apparent Rirkwood orientational correlation factor G_K. The fundamental difference between g_K and G_K stems from inclusion only in the latter of a weak macroscopic polarization contribution associated with electrostatic boundary conditions at finite distance; in the present circumstance the "boundary" is generated by the interaction cutoff. One may show (Appendix B) that

$$G_K=[9\epsilon_0/(\epsilon_0+2)(2\epsilon_0+1)]g_K. \quad (4.17)$$

For the present calculations,

$$G_K=\langle M^2\rangle/N, \quad (4.18)$$

whose value has already been presented in Eq. (4.10). If we employ the measured dielectric constant for water at 34.3°C (75.25) to compute the conversion factor shown in Eq. (4.17), the implied result is

$$g_K=2.96. \quad (4.19)$$

This agrees roughly with values that have previously been proposed; Harris, Haycock, and Alder's[34] work, for instance, implies that $g_K\cong 2.6$ at 34.3°C. It should be pointed out however that the energy rescaling of our molecular dynamics results, which is discussed in Sec. VII, improves the agreement.

D. Bond Energy Distribution

Up to this point we have frequently invoked the concept of "hydrogen bonding" to interpret those aspects of water molecule correlation which stem from the characteristic tetrahedral directionality of the effective pair potential. We now require a precise definition of "hydrogen bond," so that precise statements may be formulated about the geometrical and topological character of the random networks that exist in liquid water.

The most obvious way to define hydrogen bonds in the present circumstance uses the effective pair interaction itself. Whenever the interaction energy for a given pair of molecules lies below a negative cutoff value V_{HB}, we shall say that the pair is hydrogen bonded; if their interaction equals or exceeds V_{HB}, they are by definition not hydrogen bonded:

$$V_{\mathrm{eff}}^{(2)}(i,j)<V_{\mathrm{HB}} \quad (i,j \text{ hydrogen bonded}),$$
$$V_{\mathrm{eff}}^{(2)}(i,j)\geq V_{\mathrm{HB}} \quad (i,j \text{ not hydrogen bonded}). \quad (4.20)$$

The cutoff parameter V_{HB} is arbitrary, at least within certain limits; the fullest understanding of the nature of hydrogen-bond networks in water would result by varying this parameter and observing the consequences.

In order to identify the range of values for V_{HB} of greatest chemical relevance and interest, it is valuable to examine the entire distribution of effective pair interactions in the liquid. This interaction density, p, may be expressed in terms of the following integral:

$$p(V) = (\rho/8\pi^2) \int d\mathbf{x}_j \delta[V - V_{\text{eff}}^{(2)}(\mathbf{x}_i, \mathbf{x}_j)] g^{(2)}(\mathbf{x}_i, \mathbf{x}_j). \tag{4.21}$$

With this normalization,

$$n(V, V') = \int_V^{V'} p(V'') dV'' \tag{4.22}$$

will be the mean number of neighbors of any molecule whose instantaneous interaction with that molecule lies between V and V'. Naturally $p(V)$ will vanish if V declines below the absolute minimum of $V_{\text{eff}}^{(2)}$ noted in Eq. (2.11). One easily establishes furthermore that $p(V)$ will diverge as V^{-2} near $V=0$, owing to the preponderance of weak dipolar pair interactions at large distances.

The distribution $p(V)$ has been calculated for the molecular dynamics run and the result is displayed in Fig. 18. The expected divergence at the origin is obvious in the Figure, but it is uninteresting since it conveys no specific structural information. The primary point of interest in the curve is the large, essentially flat region in the range of V from -4.5 kcal/mole to -2.0 kcal/mole. Evidently, this reveals a wide class of moderately strong "bonds," which often suffer considerable strain. The apparent relative maximum in p(V) at about +2.5 kcal/mole we believe is a real effect, not a misleading statistical fluctuation. Probably it arises from pairs of molecules which are simultaneously bound to a third, but in such a relative configuration that they repel one another.[35]

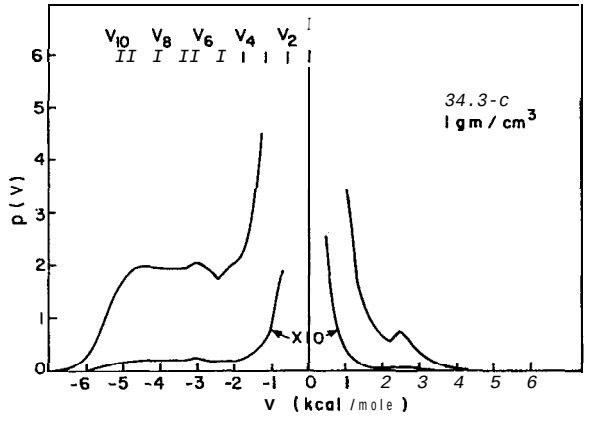

FIG. 18. Distribution function for effective pair interaction strength in water. The curves show relative numbers of molecules in successive energy intervals of width $\Delta V = 4\epsilon = 0.288$ kcal/mole.

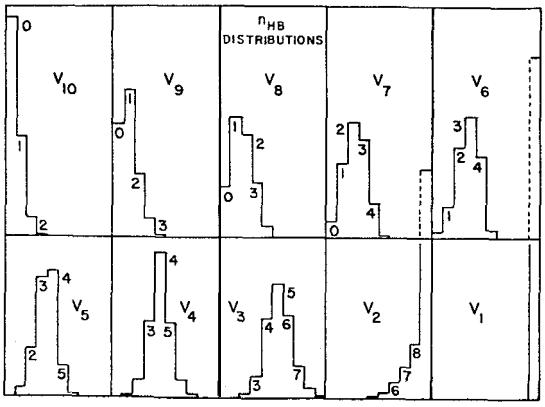

FIG. 19. Distribution of molecules according to the number of hydrogen bonds in which they engage. The set of cutoff energies V_{HB} used as alternative hydrogen-bond definitions is shown in Eq. (4.24).

On account of the negative-V plateau in p(V), it seems plausible to select V_{HB} near the middle or upper limit of this range, for example,

$$V_{HB} = -2.9 \text{ kcal/mole}. \tag{4.23}$$

This choice would certainly be consistent with the chemical suggestion that a large number of hydrogen bonds are still present in the liquid after ice is melted, without at the same time being so permissive as to include pairs of molecules much more widely separated than nearest neighbors in the ice lattice.

Using several alternative choices for V_{HB}, including the range indicated by (4.23), the concentrations of molecules engaging in different numbers of hydrogen bonds simultaneously has been calculated. This set of coordination number distributions is displayed in Fig. 19. The alternative values selected for V_{HB} are equally spaced, and have the values

$$\begin{aligned} V_j &= -8(j-1)\epsilon \\ &= -0.577(j-1) \text{ kcal/mole}, \\ j &= 1, 2, \cdots, 10. \end{aligned} \tag{4.24}$$

It is clear from Fig. 19 that these choices span a wide range of hydrogen bond definitions, from an extremely permissive limit which assigns many more than four bonded neighbors to all molecules, to a very strigent limit which makes hydrogen bonding between neighbors a rare event.

The most significant conclusion to be drawn from Fig. 19 is that as V_{HB} is varied, the coordination number distribution shifts, but it always maintains a single-maximum character. This fact alone seems to rule out the class of two-state liquid water models[26,27]

which postulate large side-by-side regions of bonded and of unbonded molecules. For such models, one would expect to observe for some V_{HB} choice a bimodal distribution with simultaneous maxima at zero and at four bonds.

It is clear from Fig. 19 that choice (4.23) for V_{HB} (essentially the value V_6) makes the most probable number of hydrogen bonds equal to three. At the same time a not insignificant number of molecules have fivefold coordination. From a detailed knowledge of $V_{eff}^{(2)}$ potential curves" it is possible to assert that essentially all molecules in ordinary ice will have precisely four bonded neighbors with choice (4.23), so the corresponding liquid phase distribution leads to a vivid picture of the nature of network disruption that accompanies melting.

It is instructive to place these bond distribution considerations for liquid water in the wider context of general liquid behavior. Thus, the anomalous character of water again stands out in comparison with the simple liquified noble gases. For liquid argon, the pair interaction distribution $p(V)$ may readily be expressed as an explicit, closed-form functional of the pair correlation function, provided V for that substance has the traditional Lennard- Jones (12-6) form. Using this hypothesis, and the argon correlation function of Fig. 4, the corresponding $p(V)$ was calculated. The result is presented in Fig. 20. Some of the obvious differences between this $p(V)$ and the one shown in Fig. 18 for water reflect the lack of rotational degrees of freedom for argon that can cause V to vary; the sharp peak at the minimum attainable V is one example. The most significant structural difference, though, is that no particularly suggestive features arise for negative V (such as a plateau region for water) that would imply a useful energy definition of "bond" between two argon atoms.

E. Stereoscopic Pictures

Intermediate configurations of the 216 water molecules, occurring every $500\Delta t = 2.1775 \times 10^{-13}$ sec, were placed on punched cards and then processed at Murray Hill to produce stereo slides. The computer program used for this purpose produces left and right eye views separately on a cathode-ray tube, whose display is then photographed with 3.5 mm film. The subsequently mounted slides can then be examined with a commercially available viewer,[36] to give a striking impression of the three-dimensional order.

The individual molecules in these pictures are rendered into stick figure form. The oxygen nucleus and the distinguishable hydrogen nucleus positions are indicated by small 0, G, and H, respectively, with the covalent bonds between them (at the tetrahedral angle) drawn as straight lines. The time interval between successive pictures is sufficiently small that the same molecule can easily be identified and followed through the entire sequence, and the motion of its individual nuclei perceived.

The inevitable immediate impression conveyed by these pictures upon first viewing is that a high degree of disorder is present. Anything else of course would make one properly suspicious that a liquid was actually being simulated. Beyond this general feature, several more detailed observations can be listed:

(1) There is a very clear tendency for neighboring molecules to be oriented into rough approximations to tetrahedral hydrogen bonds, but the average degree of bending away from bond linearity and ideal approach directions is considerable.

(2) Except on the smallest scale, the random molecular configurations are rather homogeneous in density. No large "clusters" of anomalous density seem to occur.

(3) No recognizable patterns characteristic of the known ices or clathrates appear, beyond occasional polygons of hydrogen bonds. Such polygons occur with 4, 5, 6, 7 (and perhaps more) sides, but they tend to be distorted out of their most natural conformations.

(4) Dangling OH bonds exist, which are not included in hydrogen bonds. These entities persist far longer than water molecule vibrational periods, and hence may hold the key to the structurally sensitive band shapes that arise in infrared[37] and Raman[38,39] spectroscopy of water and its solutions.

(5) No obvious separation of molecules into "network" vs "interstitial" types suggests itself. This fact is consistent with the single-peak character of the hydrogen-bond coordination number distributions exhibited in Fig. 19. It also seems to diminish the validity of the interstitial models that have been proposed to explain liquid water.[40–42]

(6) In the case of moderately well-formed (i.e., undistorted) hydrogen bonds, all angles of rotation

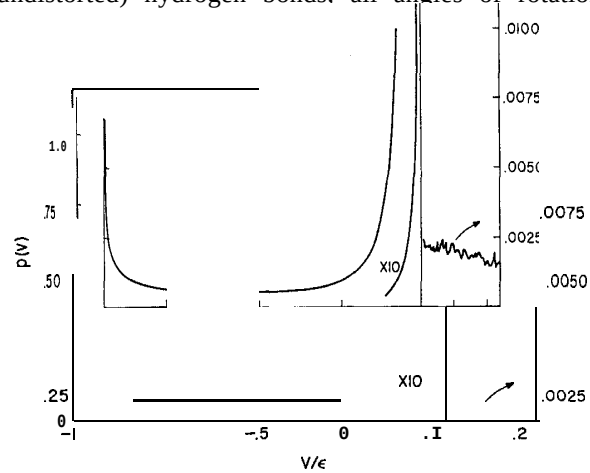

FIG. 20. Bond energy distribution for liquid Ar. The state parameters, and the correlation function employed, are those of Fig. 4.

of the molecules about the bond axis seem to be frequently represented. This behavior may have direct relevance in study of nonelectrolyte solvation, where the geometric requirements attendant upon formation of a hydrogen-bonded solvation cage forces the rotation angles into "eclipsed" configurations only,[43] thus lowering configurational entropy.

(7) No significant examples of network interpenetration were found, analogous to the interpenetration known to obtain in ice VII and ice VIII.[44]

V. KINETIC PROPERTJES

The internal structure of the water molecule requires that the static structure of the liquid be examined from many more independent points of view, for a given level of comprehension, than is required for liquid argon. This increased elaborateness persists into the regime of kinetic properties too. We now shall successively examine several aspects of the temporal development of our model water system. As in the static case, these aspects are not certainly the only informative ones that might have been chosen for study. Nevertheless, we believe that this selection serves to illuminate the dominant characteristics of water molecule motions in the liquid phase.

A. Self-Diffusion

The most obvious facet of the water molecule motions is their long time diffusion rate, which is measured by the self-diffusion coefficient $\boldsymbol{D}$. This parameter may be related, in the long time limit, to the mean-square displacement of any fixed point in a given molecule. In the case of the molecular center of mass, at position $\mathbf{R}_j(t)$ at time t,

$$D=\lim_{t\to\infty}(6t)^{-1}\langle[\mathbf{R}_j(t)-\mathbf{R}_j(0)]^2\rangle; \qquad (5.1)$$

implicit in this limit expression is a previous infinite system size limit operation.

In the molecular dynamics calculations, one naturally is limited both in time interval, and by finite system size. However, as in the case of such studies for liquid Ar,[22] the computed mean-square center-of-mass displacement appears to approach a limiting slope sufficiently rapidly that $\boldsymbol{D}$ may conveniently be extracted from the calculations. But at the same time, the molecules do not diffuse far enough to span a periodicity cell edge length, which would invalidate use of (5.1) in the present context.

Figure 21 shows the computed curve for the water molecule center-of-mass mean-square displacement. Included as well is the mean-square displacement for a proton in the liquid. At sufficiently long times, these curves would become parallel straight lines, with the proton curve displaced upward from the center of mass curve by

$$2(0.3419\sigma)^2=0.2338\sigma^2, \qquad (5.2)$$

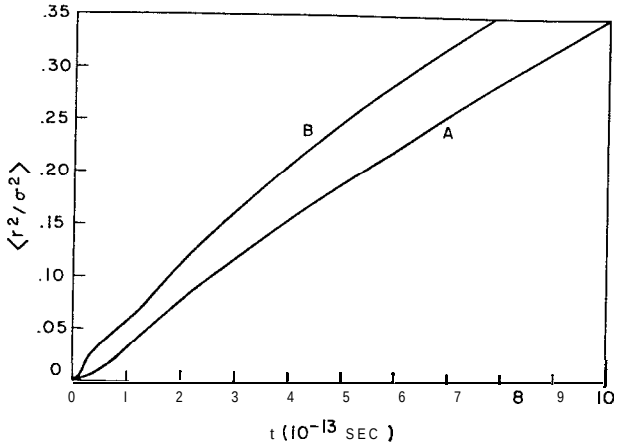

FIG. 21. Mean-square displacement of center-of-mass motion (Curve A), and of proton motion (Curve B). The apparent limiting slope of Curve A gives $D=4.2\times10^{-5}$ cm²/sec.

i.e., twice the OH bond length squared. In Fig. 21 though it is clear that the proton curve is still rising away from the essentially linear center-of-mass curve, due to the incompleteness of molecular rotation during the time allowed for computation. The motion of the center of mass therefore constitutes by far the more convenient means of estimating $\boldsymbol{D}$.

The apparent limiting slope of the center-of-mass mean-square displacement curve in Fig. 21 implies

$$\boldsymbol{D} = 4.2\text{X}\ 10^{-5}\ \text{cm}^2/\text{sec} \qquad (5.3)$$

for water at 34.3°C, and 1 g/cm³. This value is significantly larger than the value that may be inferred from recent spin-echo experiments[45,46]:

$$D=2.85\pm0.15\times10^{-5}\ \text{cm}^2/\text{sec}. \qquad (5.4)$$

But in view of the rapid variation of the experimental $\boldsymbol{D}$ with temperature, the comparison should not be viewed as unfavorable. Evidently, a small change in the energy scale of $V_{\text{eff}}^{(2)}$ could eliminate the discrepancy (see Sec. VII below).

In principle, the self-diffusion constant $\boldsymbol{D}$ could also be obtained from the velocity autocorrelation function for the molecular center-of-mass motion:

$$D=\tfrac{1}{3}\int_0^\infty \langle\mathbf{v}_j(0)\cdot\mathbf{v}_j(t)\rangle dt, \qquad \mathbf{v}_j(t)=d\mathbf{R}_j(t)/dt. \quad (5.5)$$

This velocity autocorrelation function has been computed from the molecular dynamics run, and it is shown in normalized form in Fig. 22. Since only a limited average can be performed with the run of total length 2.1775X 10^{-12} sec, this autocorrelation function necessarily represents an incomplete phase space average. The resulting statistical error is especially noticeable for "large" times (6-7X 10^{-13} sec), where the exact autocorrelation function is apparently quite small. The "cutoff" indicated in Fig. 22 at

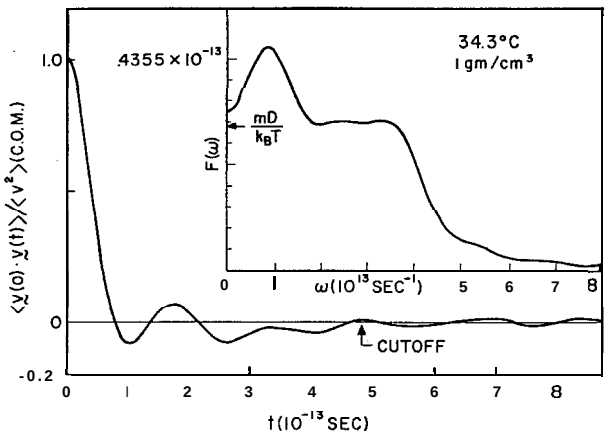

FIG. 22. Center-of-mass velocity autocorrelation function (normalized at $t=0$) for water and its Fourier cosine transform. The "cutoff" locates approximately the point beyond which statistical noise dominates the autocorrelation function.

4.78×10^{-13} sec represents our estimate of the point beyond which the curve is primarily statistical noise. At shorter times, though, the autocorrelation curve shown is probably a reasonably accurate approximation to the exact function.

Figure 22 also presents the Fourier transform[47]

$$F(\omega) = \int_0^\infty \frac{\langle \mathbf{v}(0)\cdot\mathbf{v}(t)\rangle}{\langle \mathbf{v}(0)\cdot\mathbf{v}(0)\rangle}\cos(\omega t)\,dt. \qquad (5.6)$$

In principle, one should have

$$F(0) = mD/k_BT; \qquad (5.7)$$

however, this identity is not quite obeyed using the D value in Eq. (5.3), as the arrow on the $F(\omega)$ scale shows. The discrepancy reflects the magnitude of errors in the incomplete phase averages involved in both methods of evaluating D. This suggests that the D value shown in Eq. (5.3) may be in error by as much as 10%, compared to the model's precise self-diffusion constant at 34.3°C and 1 g/cm³.

Even accounting for the statistical uncertainty present in the center-of-mass velocity autocorrelation in Fig. 22, it is obvious that the average molecular motion is relatively oscillatory. Once again our water model stands in distinct contrast to liquid Ar, for which Fig. 23 presents the velocity autocorrelation function. For this comparatively simple liquid, the autocorrelation has only a single well-defined negative minimum, followed by a slow rise to zero. The hydrogen bonding in liquid water, however, produces a more persistently oscillatory motion, as a result of greater structural rigidity.

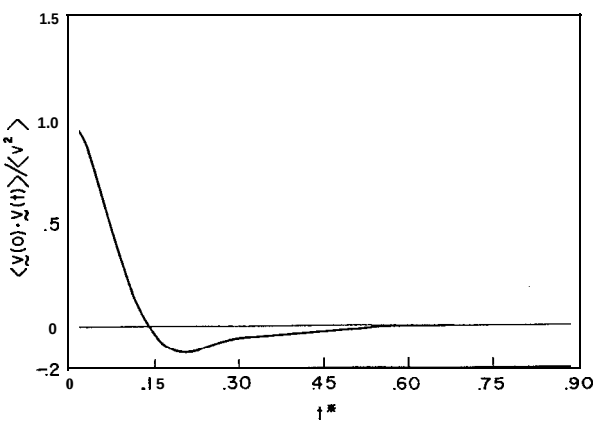

FIG. 23. Normalized velocity autocorrelation function for liquid argon; $\rho^*=0.81, T^*=0.74$. The reduced time t^* is measured in units $\sigma(m/\epsilon)^{1/2}$.

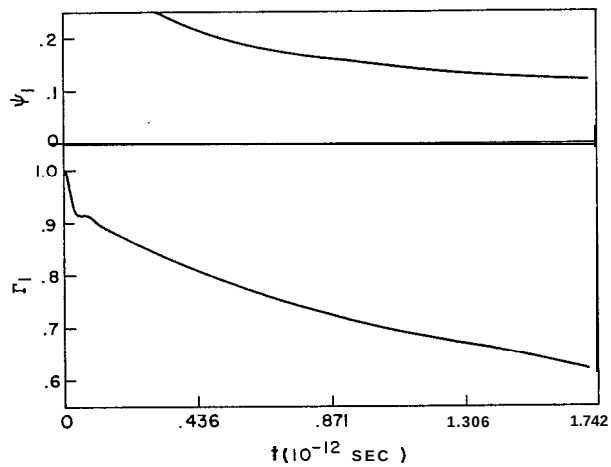

FIG. 24. Dipole direction relaxation function $\Gamma_1(t)$. The related $\psi_1(t)$ is defined in Eq. (5.9).

The stereo pictures of intermediate configurations are too widely separated in time (2.1775×10^{-13} sec) to resolve proton oscillations with great detail. However, they do suffice to give an idea of why and how translational diffusion proceeds. The hydrogen bonds between neighboring molecules are continually subject to varying degrees of strain. Accordingly, each molecule is tugged around in a random fashion by its imperfectly aligned neighbors, while at the same time those neighbors are also being forced to rearrange by *their* neighbors. In this circumstance, it is frequently the case that hydrogen bonds become strained to the breaking point; i.e., it is favorable for a molecule to reorient to form new hydrogen bonds to other nearby molecules. The amplitude of these very anharmonic motions is sufficiently high at the ambient temperature that settling down into a regular and relatively unstrained arrangement is overwhelmingly unlikely.

There are effectively so many available highly strained configurations near to one another, that their interconversion is a continual, rather than a discrete, process. There is no evidence in the stereo pictures

for a hopping process between alternative positions of mechanical stability. Instead, translational diffusion proceeds via individual molecule participation in the continual restructuring of the labile random hydrogen-bond network.

B. Dipole Direction Relaxation

The forces of hydrogen bonding between molecules prevent rapid turning over of those molecules. The autocorrelation function for the dipole direction of a given molecule

$$\Gamma_1(t) = \langle \boldsymbol{\mu}_j^{(1)}(0)\cdot\boldsymbol{\mu}_j^{(1)}(t)\rangle \equiv \langle P_1[\cos\theta_j(t)]\rangle \quad (5.8)$$

clearly shows this rotational retardation. It is plotted in Fig. 24 both in direct form, as well as logarithmically in terms of the quantity

$$\psi_1(t) = -(10^3\Delta t/t)\ln\langle P_1[\cos\theta_j(t)]\rangle. \quad (5.9)$$

After a brief period of initial libration lasting roughly 10^{-13} sec, a long monotonic decay ensues which apparently persists well beyond the time limit imposed by the computation. By fitting a simple exponential function to Γ_1 in the monotonic range, one infers a longest relaxation time τ_1 equal to about 5.6×10^{-12} sec.

It has been claimed[48,49] that the macroscopic dielectric relasation time (for polar liquids with large ϵ_0) should be $\frac{3}{2}$ or 2 times as large as τ_1. Our calculations would then imply for water at 34.3°C:

$$8.4\times10^{-12}\,\text{sec} \leq \tau_d \leq 11.2\times10^{-12}\,\text{sec}. \quad (5.10)$$

The measured dielectric relaxation time at this temperature is[50]

$$\tau_d = 6.7\times10^{-12}\,\text{sec}, \quad (5.11)$$

so taking the various imprecisions into account, our water model seems not to be too far out of line.

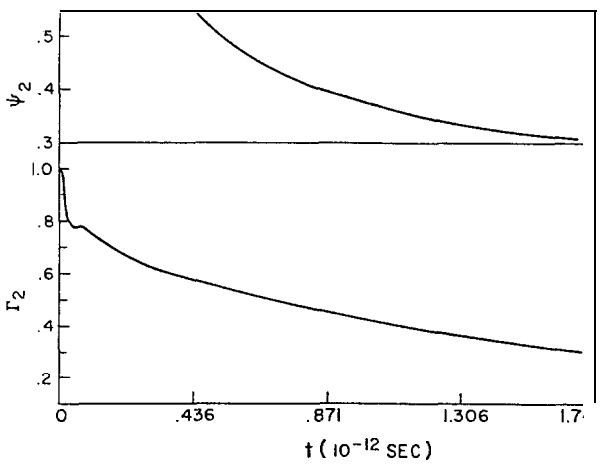

FIG. 25. Relaxation function $\Gamma_2(t)$ for the dipole direction second harmonic. The related function $\psi_2(t)$ is defined in Eq. (5.14).

The autocorrelation function $\Gamma_1(t)$ may be regarded as the leading member of an infinite sequence of autocorrelation functions for spherical harmonics of ascending order:

$$\Gamma_l(t) = \langle P_l[\boldsymbol{\mu}_j^{(1)}(0)\cdot\boldsymbol{\mu}_j^{(1)}(t)]\rangle, \quad (5.12)$$

where P_l is the lth Legendre polynomial. If the unit dipole direction vector $\boldsymbol{\mu}_j^{(1)}$ moved in time by a true rotational Brownian motion, the Γ_l would decay exponentially with relaxation times τ_l all simply related to τ_1:

$$\tau_l = 2\tau_1/l(l+1). \quad (5.13)$$

In order partially to test this possibility, $\Gamma_2(t)$ was evaluated for the present water model, along with the $l=2$ analog of ψ_1:

$$\psi_2(t) = -(10^3\Delta t/t)\ln\Gamma_2(t). \quad (5.14)$$

These two functions are plotted in Fig. 25. Again an initial rapid libration shows up, followed by a longer monotonic decay. This monotonic portion is certainly not precisely characteristic of a single exponential decay, but indicates that the most persistent component exhibits a relaxation time

$$\tau_2 \cong 2.1\times10^{-12}\,\text{sec}. \quad (5.15)$$

The ratio of $l=1$ to $l=2$ relaxation times for the water model computation is therefore somewhat less than the ideal Brownian motion ratio 3:

$$\tau_1/\tau_2 \cong 2.7. \quad (5.16)$$

This diminution should be expected however, since the water molecule rotational motion corresponds more closely to a sequence of finite stochastic jumps, rather than to the infinitely rapid infinitesimal jumps implied by classical Brownian motion (Wiener process[51]).

The nuclear magnetic resonance spin-lattice relaxation time T_1 contains a contribution, due to molecular rotation, that in principle measures $\Gamma_2(t)$ if the rotation is isotropic.[52] Krynicki[53] has inferred from his T_1 measurements how τ_2 should vary with temperature; his results imply that

$$\tau_2 \cong 1.9\times10^{-12}\,\text{sec}. \quad (5.17)$$

In view of the several uncertainties involved in interpretation of the experiments, the τ_2 values (5.15) and (5.17) are in satisfactory agreement.

C. Dielectric Relaxation

The autocorrelation $\Gamma_1(t)$ is central to the frequency dependence of the liquid's dielectric constant. We have already noted (Sec. IV. C) that ignorance of the correct liquid-phase molecular dipole moment limits one's ability to predict the static dielectric constant ϵ_0. This ignorance naturally hinders full understanding of $\epsilon(\omega)$ as well, as does the present lack

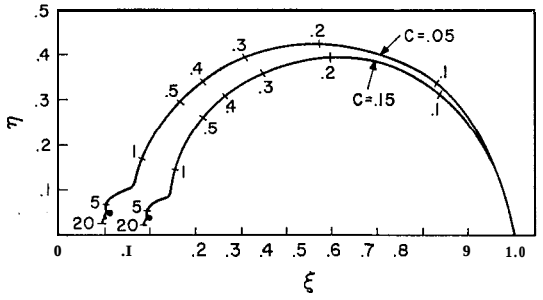

FIG. 26. Cole-Cole plots for the frequency-dependent dielectric constant e(w). The curves are based upon the Nee–Zwanzig theory, Ref. 49. The reduced coordinates are defined by Eq. (5.19), and c defined by Eq. (5.20). Marks on the curves indicate frequency in units 10^{12} sec^{-1}.

of a fully general theory of time-dependent dielectric response in polar fluids.

Nevertheless, the recent approximate analysis of dielectric relaxation by Nee and Zwanzig[49] provides a convenient tentative basis on which to convert our molecular dynamics results into traditional Cole-Cole plots.[54] They derive the following relation:

$$\frac{\epsilon_0[\epsilon(\omega)-\epsilon_\infty][2\epsilon(\omega)+\epsilon_\infty]}{\epsilon(\omega)(\epsilon_0-\epsilon_\infty)(2\epsilon_0+\epsilon_\infty)} = -\int_0^\infty dt \exp(i\omega t)\,\frac{d\Gamma_1(t)}{dt}\,; \tag{5.18}$$

for present purposes the high-frequency dielectric constant ϵ_∞ corresponds to about the 10-cm^{-1} wavelength region, which has been reported[55] to yield an ϵ_∞ of 4.5 for water.

By using the previously evaluated $\Gamma_1(t)$ and a simple exponential extrapolation beyond the range shown in Fig. 24, it is possible to evaluate $\xi(\omega)$ and $\eta(\omega)$, the real and imaginary parts of $\epsilon(\omega)/\epsilon_0$:

$$\epsilon(\omega)/\epsilon_0 = \xi(\omega) + i\eta(\omega), \tag{5.19}$$

from expression (5.18). The precise value of

$$c = \epsilon_\infty/\epsilon_0 \tag{5.20}$$

for our specific model is unknown, but if real water at 34.3°C gives a reliable indication, it should be roughly 0.06.

Figure 26 shows the Cole-Cole plots obtained for the c values 0.05 and 0.15. The curves are rather close to the classic semicircular shape for $\omega < 2\text{X}\,10^{-12}$ sec^{-1}. However for high frequencies, "curlicues" appear which may be attributed to the rapid initial librational motion in $\Gamma_1(t)$.

D. Proton Motion and Neutron Scattering

Owing to the fact that protons are strong incoherent scatterers, cold neutron scattering provides a convenient experimental tool for the study of single proton motions in water. It is therefore important to extract information from the molecular dynamics computation that bears specifically on these motions. There are in fact several independent dynamical quantities that deserve attention, beyond the mean-square displacement that has already been considered.

The angular velocity autocorrelations about the three principle axes of the molecule:

$$\langle \omega_\alpha(0)\omega_\alpha(t)\rangle/\langle \omega_\alpha^2\rangle, \qquad \alpha = 1, 2, 3, \tag{5.21}$$

illustrate one aspect of proton motion. Figure 27 presents these three rapidly decaying functions. All three indicate a substantial librational, or oscillatory, character. The rates of libration are in the same order as the reciprocals of the respective moments of inertia:

$$I_2^{-1} > I_3^{-1} > I_1^{-1}; \tag{5.22}$$

as the insert in Fig. 27 indicates, axis 1 is perpendicular to the molecular plane, axis 2 is in the molecular plane, and axis 3 is the twofold molecular symmetry axis.

A magnified view of the initial portion of $\Gamma_1(t)$ (shown previously in Fig. 24) is also included in Fig. 27. Only rotations about axes 1 and 2 affect the dipole direction $\mu_j^{(1)}$ for molecule j, so it is a combination of these two motions which affects Γ_1. Since the librational rates are distinctly different about these two "dipole active" axes, we-see why the com-

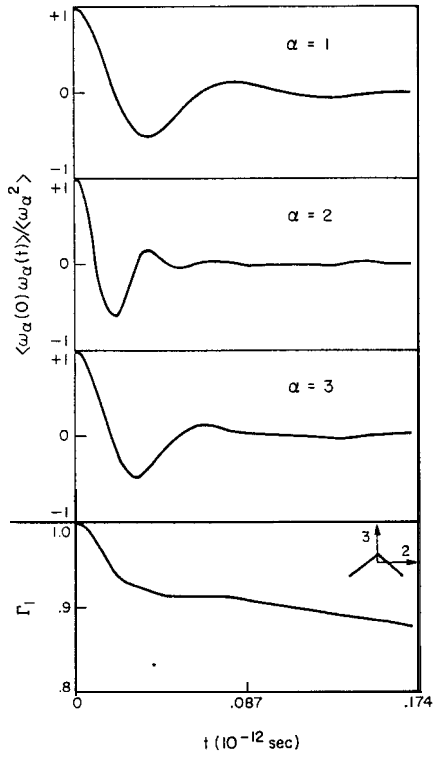

FIG. 27. Angular velocity autocorrelation functions. Included for comparison (bottom) is the initial behavior of $\Gamma_1(t)$, shown earlier in Fig. 24. The principal axis numbering is shown in the insert.

bination in Γ_1 exhibits the oscillatory character less vividly than the ω_α autocorrelations themselves.

The spectral resolutions, or Fourier transforms, of the ω_α autocorrelations are defined thus:

$$f_\alpha(\Omega) = \int_0^\infty \frac{\langle \omega_\alpha(0)\omega_\alpha(t)\rangle}{\langle \omega_\alpha^2\rangle}\cos(\Omega t)\,dt. \qquad (5.23)$$

They are shown in Fig. 28. The positions of their respective maxima and centroids again reflect the ordering of librational rates according to the inertial moments.

The autocorrelation of the total angular velocity for a given molecule,

$$\langle \boldsymbol{\omega}(0)\cdot\boldsymbol{\omega}(t)\rangle / \langle |\boldsymbol{\omega}|^2\rangle, \qquad (5.24)$$

may be obtained from a linear combination of the separate normalized autocorrelations (5.21), using weights that follow from the thermal equilibrium conditions,

$$\langle \omega_\alpha^2\rangle = k_B T/I_\alpha. \qquad (5.25)$$

The resulting spectrum, $f_{tot}(\Omega)$, that follows from (5.24) is presented in Fig. 29.

If the vector $\boldsymbol{\varrho}$ denotes the position of a given proton relative to the center of mass of the molecule containing it, then the velocity of that proton measured relative to the center of mass will be

$$\boldsymbol{\omega}\times\boldsymbol{\varrho}, \qquad (5.26)$$

where $\boldsymbol{\omega}$ is that molecule's angular velocity. Since our water model molecules are completely rigid, the length $|\boldsymbol{\varrho}|$ remains fixed so that the proton seems to be moving on a spherical surface when viewed from the center of mass. The appropriate normalized velocity autocorrelation function for description of proton diffusion on the sphere is the following:

$$\phi(t) = \langle [\boldsymbol{\varrho}(0)\times\boldsymbol{\omega}(0)]\cdot[\boldsymbol{\varrho}(t)\times\boldsymbol{\omega}(t)]\rangle / \langle |\boldsymbol{\varrho}\times\boldsymbol{\omega}|^2\rangle, \qquad (5.27)$$

and we shall represent its spectral resolution in the usual way:

$$\Phi(\Omega) = \int_0^\infty \phi(t)\cos(\Omega t)\,dt. \qquad (5.28)$$

The Fourier transform Φ may be related to the time dependence of the mean square of $\mathbf{u}$, the proton displacement relative to the center of mass. Specifically, it is easy to establish that

$$\langle |\mathbf{u}(t)|^2\rangle = \left(\frac{4}{\pi}\right)\langle |\boldsymbol{\varrho}\times\boldsymbol{\omega}|^2\rangle \int_0^\infty \left(\frac{1-\cos(\Omega t)}{\Omega^2}\right)\Phi(\Omega)\,d\Omega. \qquad (5.29)$$

Since the spherical surface upon which the proton must move is bounded, this last quantity must approach a finite limit as $t\to\infty$. Hence $\Phi(0)$ must vanish, and the integral

$$\int_0^\infty \Omega^{-2}\Phi(\Omega)\,d\Omega \qquad (5.30)$$

is constrained to a value set by simple geometrical considerations.

The functions $\phi(t)$ and $\Phi(\Omega)$ obtained from the molecular dynamics are shown in Fig. 30. The former demonstrates once again the substantial oscillatory component of proton motion. To evaluate $\Phi(\Omega)$ numerically from $\phi(t)$, an integration cutoff time had to be imposed, which is indicated in Fig. 30 by an arrow. The resulting numerical $\Phi(\Omega)$ fails to vanish at the origin, due to absence of a long time negative tail in $\phi(t)$ that is associated with the eventual ($\approx 5\times$

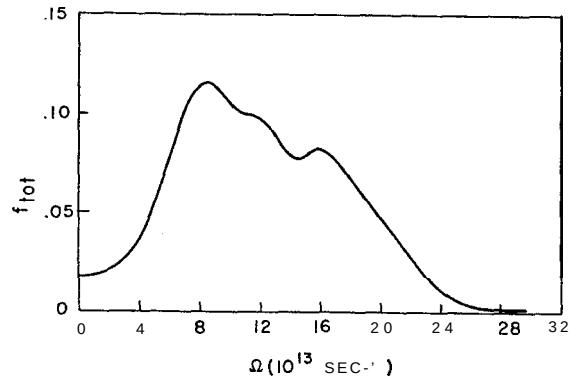

FIG. 29. Frequency spectrum of the total angular momentum autocorrelation function.

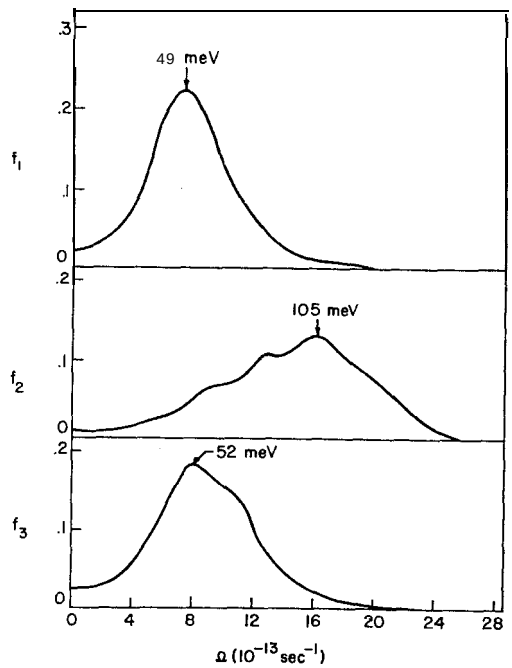

FIG. 28. Frequency spectra of the angular velocity autocorrelation functions.

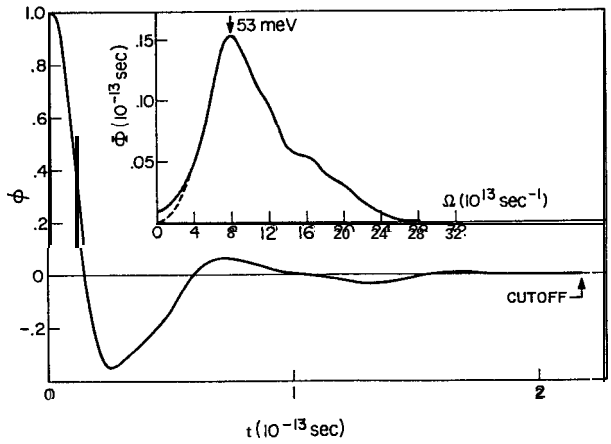

FIG. 30. Normalized velocity autocorrelation function (and its frequency spectrum) for proton motion relative to the center of mass.

10^{-12} sec) **turning over of molecules, The dashed curve** shown for Φ near the origin represents our estimate of how the accurate Φ (incorporating the effect of the negative ϕ tail) would have to behave, including the fact that integral (5.30) is fixed.

The central quantity probed by neutron inelastic scattering from water is the Van Hove[56] self-correlation function $G_s(r,t)$ for protons. This function gives the spatial distribution at time t (in an ensemble of identically prepared systems) for a proton initially at the measurement origin when $t=0$. Its spatial Fourier transform in the classical limit is given by

$$F_s(k,t) = \langle \exp\{i\mathbf{k}\cdot[\mathbf{r}(t)-\mathbf{r}(0)]\}\rangle. \qquad (5.31)$$

A substantial body of theoretical effort has been devoted to understanding these self-correlation functions in general liquids. A particularly popular approach, the "Gaussian approximation,"[57] has been motivated by the nature of the macroscopic diffusion process. This approximation requires $G_s(r,t)$ to be a Gaussian function in r at all times, with a width chosen to reproduce the correct microscopic mean-square displacement $\langle|\mathbf{r}(t)|^2\rangle$. The equivalent requirement is that $F_s(k,t)$ have the form

$$F_s(k,t) = \exp[-\tfrac{1}{6}k^2\langle r^2(t)\rangle]. \qquad (5.32)$$

Our molecular dynamics calculation enables us to test the validity of Eq. (5.32) directly, since independent calculations of $\langle r^2(t)\rangle$ and of expression (5.31) are possible. Figure 31 graphically shows the test of Eq. (5.32) for three wave vector choices that are consistent with the periodicity cube employed in the dynamics

$$k\sigma = 9.517,\ 14.276,\ 19.034. \qquad (5.33)$$

Although the specific Gaussian approximation (5.32) accounts qualitatively for the behavior of $F_s(k,t)$, it is obvious that substantial quantitative errors arise. For each wave vector, the Gaussian $F_s(k,t)$ decays too rapidly to zero with increasing t in Fig. 31. If one were to force neutron scattering measurements to fit expression (5.32) in this k range, the apparent $\langle r^2(t)\rangle$ would increase too slowly with t; i.e., the apparent self-diffusion constant would be anomalously small.

The failure of approximation (5.32) for intermediate k values is connected to the fact that the Van Hove function $G_s(r,t)$ is not itself Gaussian in r for intermediate times.[58] It is worth recalling that a distinctly non-Gaussian $G_s(r,t)$ has also been found in molecular dynamics calculations on liquid argon.[22]

The fact that the actual $F_s(k,t)$ curves in Fig. 31 decay in time more slowly than their Gaussian analogs is related to the narrowing that has been observed in water for neutron quasielastic scattering peaks.[59,60] One conceivable way in which this narrowing could be explained would be a jump diffusion mechanism, whereby molecules would execute occasional hops of considerable length between quasicrystalline sites of oscillation in the liquid. Indeed theories of precisely this character have been advanced to explain the neutron experiments by Singwi and Sjölander,[61] and Chudley and Elliot.[62] The former authors conclude for example that at 20°C each water molecule oscillates in place for about 4×10^{-12} sec before experiencing rapid diffusion (a "jump") to a new position of oscillation.

In confronting a phenomenon as complicated as proton motion in liquid water must surely be, one runs the risk that experimental data such as neutron scattering can be explained in a variety of ways. Thus, it may be that a jump diffusion mechanism is

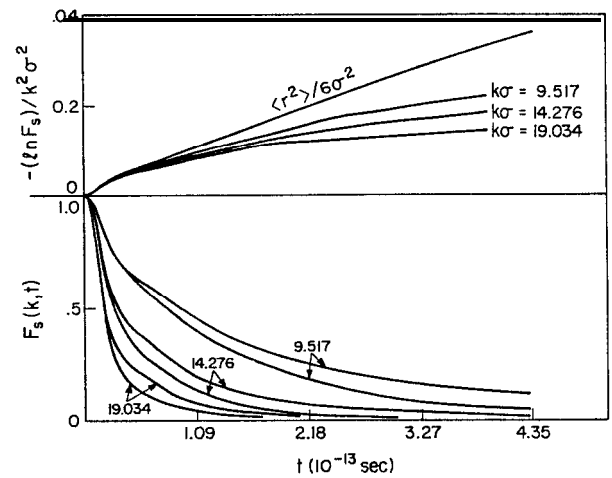

FIG. 31. Spatial Fourier transform $F_s(k,t)$ of the Van Hove self-correlation function for protons. Curves for the three values $k\sigma=9.517$, 14.276, 19.034 are shown. In the lower graph, the Gaussian approximation (5.32) gives the lower curve for each pair. In the upper logarithmic plot, the Gaussian approximation curves are coincident ($\langle r^2\rangle/6\sigma$).

sufficient to esplain that data, but not logically necessary. In fact, the jump diffusion mechanism definitely conflicts with our molecular dynamics results. Both the temporal correlations, and the sequence of stereo pictures, show that well-defined quasicrystalline sites of residence do not exist in liquid water. The diffusive molecular motions are much more continuous and cooperative and apparently depend strongly upon the distinctive liquid-phase random hydrogen-bond network that is present and forever transforming its topological character.

Sakamoto *et al.*[63] have computed proton mean-square displacements vs time by Fourier-transforming neutron scattering data. Although their results have been interpreted as further support for the jump diffusion mechanism[64] such an interpretation is subject to esnctly the same uniqueness criticism. For the diffusion times probed by the analysis of Sakamoto *et al.* (2×10^{-13} to 10^{-11} sec), the mean-square proton displacements are similar to those shown in Fig. 21 for the molecular dynamics. In this time range, the only clear distinctive feature exhibited by both approaches is that the proton displacement curve lies *above* the straight line passing through the origin with slope corresponding to the correct D. In order to effect a discriminating experimental test of diffusion mechanisms in liquid water, sufficient improvement in experimental technique is required to examine times of the order of 10^{-14} sec accurately.

As a final aspect of water molecule kinetics, we mention that the velocity autocorrelation for protons (within present accuracy) is found to be the sum of the molecular center-of-mass autocorrelation (Fig. 22), and the "motion on the sphere" autocorrelation (Fig. 30). Thus the translational and rotational motions of the molecules seem to proceed independently of one another, on the average. Figure 32 therefore exhibits the total proton motion spectrum that was obtained by linear combination of the spectra reported in Figs. 22 and 30.

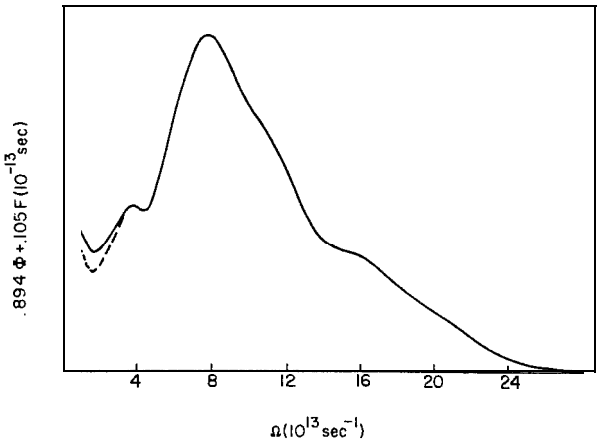

FIG. 32. Frequency spectrum for proton total velocity autocorrelation function. As the legend indicates, this was obtained as a linear combination of the spectra in Figs. 22 and 30.

VI. TEMPERATURE VARIATIONS

In addition to the one temperature studied at length in this paper, 34.3°C, our water model needs and deserves to be examined at several other temperatures to allow instructive comparisons to be carried out. These extensions are, in fact, underway and will be reported in due course. For the present, we shall only briefly mention a low temperature run to add perhaps some more credibility to our water model.

This new run involved the same condition as its predecessor ($N = 216$, 18.62 8 cubical box with periodic boundary conditions), but the temperature was only 265°K (−8.2°C). The system therefore corresponded to liquid water in a state of moderate supercooling, but under the circumstances that prevail, essentially no chance existed for the liquid to nucleate and freeze into ice. The run lasted 4000 Δt.

The osygen-nucleus pair correlation function $g_{OO}^{(2)}(Y)$ computed for this lower temperature superficially resembles the one shown in Fig. 3. It approaches unity with increasing r rapidly enough again to exclude bulky "clusters" or "icebergs" from serious consideration. Furthermore, the distance ratio for second and first peaks is rather close to the ideal value for tetrahedral hydrogen bonding. However, the first maximum of $g_{OO}^{(2)}(r)$ is significantly larger (2.97, compared to 2.56 in Fig. 3) and the succeeding minimum deeper. The second maximum appears to be better developed and narrower. Evidently the random hydrogen-bond network has tightened up considerably, by discriminating against severe distortions of the ideal tetrahedral coordination geometry.

The stereo pictures that have been produced from this lower temperature run bear out that conclusion. The hydrogen bonds that form between neighboring molecules appear to be more nearly linear and to observe the tetrahedral angles of approach more frequently. Although the bonds in the random network tend to strengthen at lower temperature, this does not imply that it is easier then to identify a few "interstitial" molecules; as before we see no clear examples of any interstitials. Also, the liquid seems to show no marked tendency anywhere to organize the beginnings of ice nuclei.

To the extent that x-ray scattering experiments predominately reflect $g_{OO}^{(2)}(r)$, our structural shifts with temperature variation agree qualitatively with measurements reported by Narten, Danford, and Levy.[29]

Naturally the strengthening of the interactions tends to slow down molecular diffusive motions markedly. The self-diffusion constant D at 265°K is found to be approximately 1.5×10^{-5} cm²/sec for the molecular dynamics simulation. Once again this seems to be rather larger than the experimental value 0.75±

0.03×10^{-5} cm²/sec,[65] but comparison of the ratio of values at -8.2 and 34.3°C (0.36 theoretical, 0.26 experimental) indicates roughly the necessary rapid temperature variation for D. Furthermore, the simple energy rescaling discussed in the following section induces far better agreement with the measured D values at both rescaled molecular dynamics temperatures.

In order to round out the study of temperature variations, we intend to study our model up to the neighborhood of the critical temperature (374°C). This should provide a comprehensive account of the thermal disruption of the hydrogen-bond network, and should permit a reasonably accurate evaluation of the constant volume heat capacity.

VII. DISCUSSION

In order to continue systematically applying the molecular dynamics method to water, two types of extensions of the present work are necessary. The first involves expanding the domain of application of the model employed here to include a wide range of densities and of temperatures (mentioned in the preceding section), as well as to include solvation and interface studies. The second type of extension is the analysis of ways in which the effective pair interaction $V_{\text{eff}}^{(2)}$ should be modified to yield a more accurate description of real water. These two aspects need to be carried forward in parallel, since accurate determination of the properties implied by a given Hamiltonian, in comparison with experimental results, provides the basis for modification.

With respect to future study of aqueous solutions, it should be mentioned that the model employed in this paper can be immediately adapted to simulation of a particularly simple solute. By retaining only v_{LJ} [see Eq. (2.5)] in the effective pair interaction between a chosen molecule and all the others, that molecule should reasonably well behave as a neon atom if in addition the full mass were placed at its center. This single solute particle of course could not hydrogen bond to its neighbors. One would then be particularly interested to see if the surrounding water molecules organized themselves into a sort of "cage" analogous to those present in clathrates. The results would be especially interesting in view of the "hydrophobic bond" concept that has been proposed to explain the interaction of nonpolar solutes in water.[66,67]

In order to broaden the scope of solution studies to include other solutes, information will be required about the interaction of water molecules with a variety of ions and molecules. Extensive quantum mechanical calculations would have considerable value in determining characteristic shapes of potential surfaces for water molecules in interaction with distinct chemical groupings, e.g., methyl groups, carbonyl groups, hydroxyls, conjugated double bonds between carbon atoms, amines, etc. With such information in hand, it would become possible to design molecular dynamics calculations to study the hydration of biological macromolecules and the interaction of water with membranes.

The simplest of all possible modifications that might be applied to the effective potential would be the strength rescaling mentioned briefly at the end of Sec. III. If one were to choose the interaction energy $\langle V_N \rangle / N$ and the self-diffusion constant D as having central importance, then a rescaling factor

$$1+\zeta = 1.06 \tag{7.1}$$

would have the effect of changing the temperature to 52.8°C, while inducing much better agreement than previously between calculations and experiment both for mean interaction energy:

$$\langle V_N \rangle / N = -9.735 \text{ kcal/mole (molecular dynamics rescaled)},$$
$$= -9.63 \text{ kcal/mole (exptl, 52.8°C)}, \tag{7.2}$$

and for the self-diffusion constant:

$$D = 4.3 \times 10^{-5} \text{ cm}^2/\text{sec (molecular dynamics rescaled)},$$
$$= 4.1 \times 10^{-5} \text{ cm}^2/\text{sec (exptl, 52.8°C)}. \tag{7.3}$$

At the same time, of course the rotational relaxation times τ_1 and τ_2 would decrease by $(1+\zeta)^{1/2}$, making them apparently agree better with experiment. But since the theoretical frameworks are weak in which τ_1 and τ_2 are related to dielectric and NMR experiments, this agreement should probably be given relatively little weight at present.

Energy rescaling also affects the value predicted by molecular dynamics for the Kirkwood orientational correlation factor. When the measured ϵ_0 for water at 52.8°C is inserted in Eq. (4.17) to convert G_K to g_K, one obtains

$$g_K = 2.72, \tag{7.4}$$

somewhat smaller than the "unscaled" result 2.96 in Eq. (4.19). The previously cited work of Harris, Haycock, and Alder,[34] which suggests g_K should be in the range 2.5-2.6 at this temperature, also supports the rescaling.

The same energy rescaling factor 1.06 seems tentatively also to produce considerable improvement in agreement with experiment for the low temperature run mentioned in the preceding Section. Although the nominal temperature 265°K (−8.2°C) for that run corresponded to supercooled water, the rescaled temperature 280.9°K (7.7°C) lies above the melting point of ice. Eventually, it would be very interesting to carry out a molecular dynamics simulation on a

strongly supercooled water sample (even on the rescaled basis), to see what type of local order arises.

Beside the strength rescaling for $V_{\text{eff}}^{(2)}$, a length rescaling is also possible. This would produce a shift in density (rather than temperature) and would require reinterpretation of all quantities dependent upon the length unit. At present no compelling evidence motivates such a distance rescaling.

Probably the principal criticism which might be directed toward our choice for $V_{\text{eff}}^{(2)}$ is that it is somewhat too "tetrahedral." However, it is significant to have observed that even in the presence of this tetrahedral bias, the local structure produced in our model "water" still manifests very substantial randomness, and fails to mimic known crystal structures. It is therefore quite unlikely that a less tetrahedral $V_{\text{eff}}^{(2)}$, at a given temperature, would be more successful in building liquid-phase networks akin to the ice lattice or the clathrates at the local level.

Barker and Watts[68] have carried out a Monte Carlo calculation for $N=64$ water molecules (at 25°C), using the Rowlinson[69] pair potential. Like our own effective pair potential, the Rowlinson interaction is based on a four-point charge complex for each molecule. However, the positions of these charges do not lead to a natural tetrahedral arrangement of neighbors. As a result, the computed oxygen-nucleus pair correlation function tends to have a rather large number of nearest neighbors (6.4 out to distance 3.5 Å), and the positions of first and second maxima are far from the ideal tetrahedral ratio. Although the Rowlinson potential may provide a reasonable account of the interaction for isolated pairs of water molecules in the vapor, it probably deviates too far from the tetrahedral directionality required of a condensed phase $V_{\text{eff}}^{(2)}$ that must lead to essentially universal fourfold coordination in aqueous crystals.

A possible modification of our own $V_{\text{eff}}^{(2)}$, Eq. (2.5), which does not seriously compromise its directionality, would be to shorten the distance from the oxygen nucleus to the *negative* point charges, without changing any angles or the distance to the positive charges. At the same time it would be necessary to adjust the parameters η, R_L, and R_U, to maintain the strength and length of undistorted hydrogen bonds. This change would permit greater freedom in approach direction for formation of linear hydrogen bonds. The mean interaction energy in the liquid should thereupon increase in magnitude. It must be left for future investigation, however, to determine what the concomitant effects on static correlation functions and kinetic properties would be.

ACKNOWLEDGMENT

The authors are indebted to Dr. Seymour H. Koenig, IBM Watson Laboratory, for arranging a generous grant of computer time at the IBM Computation Center to carry out the low temperature run reported briefly in Sec. VI.

APPENDIX A

Given $\mathbf{x}_i$ and $\mathbf{x}_j$ [see Eq. (3.1)] and the positions of the oxygen and four point charges in each molecule, we can calculate the list of 17 distances: r_{ij}, the oxygen-oxygen distance; and 16 point charge distances $d_{\alpha_i\alpha_j}$. Then $V_{\text{eff}}^{(2)}$ gives rise to a force vector of magnitude:

$$24(\epsilon/r_{ij})[2(\sigma/r_{ij})^{12}-(\sigma/r_{ij})^{6}] -6[(r_{ij}-R_L)(R_U-r_{ij})/(R_U-R_L)^3]v_{\text{el}}(\mathbf{x}_i,\mathbf{x}_j) \quad \text{(A1)}$$

acting between the two oxygen nuclei. The term with v_{el} [Eq. (2.8)] is present only for $R_L \leq r_{ij} \leq R_U$ [see Eq. (2.9)].

Each pair of point charges in the respective molecules gives a force vector of magnitude

$$S(r_{ij})\ (0.19e)^2(-1)^{\alpha_i+\alpha_j}/d_{\alpha_i\alpha_j} \quad \text{(A2)}$$

acting between that pair.

The Cartesian components of these forces are obtained simply by multiplying the magnitudes by ratios of the type $(x_{0i}-x_{0j})/r_{ij}$ and $(x_{\alpha_i}-x_{\alpha_j})/d_{\alpha_i\alpha_j}$.

These 17 forces then give, by a summation of respective components, the total body force acting on a molecule. Using the transformation matrix which rotates xyz into $x'y'z'$ (Fig. 2), the components of the torque $\mathbf{N}_j$ [Eq. (3.5)] can also be calculated from the components of the force acting on each of the five points of a molecule (the positions of the oxygen nucleus and the four point charges). Adding the inertial terms [Eq. (3.6)] gives the derivatives of the angular velocities about the principal axes of inertia.

To indicate the scheme[70] we have used for solving the Newton-Euler equations of motion, we shall take the following three differential equations as prototypes for Eqs. (3.3), (3.6), and (3.7), respectively,

$$\begin{aligned} d^2x/dt^2 &= f(x, p), \\ dq/dt &= g(x, p, q), \\ dp/dt &= h(p, q). \end{aligned} \quad \text{(A3)}$$

Here x typifies center of mass Cartesian coordinates, q is the angular velocities about the principal axes of inertia, and p is the Euler angles.

The problem is to get x, p, q at $t+\Delta t$ knowing the values at time t. Assume that the calculation has already been initiated so that, apart from x, p, q at t, *we also* know the first five derivatives of x and the first four of p and q. Let x_n, e.g., denote

$$[(\Delta t)^n n!]d^nx/dt^n.$$

We predict the values of all these quantities at $t+\Delta t$ by using the Pascal triangle:

$$x_0' = x_0 + x_1 + x_2 + x_3 + x_4 + x_5,$$
$$x_1' = x_1 + 2x_2 + 3x_3 + 4x_4 + 5x_5,$$
$$x_2' = x_2 + 3x_3 + 6x_4 + 10x_5,$$
$$x_3' = x_3 + 4x_4 + 10x5,$$
$$x_4' = x_4 + 5x_5, \qquad \text{(A4)}$$

and similarly for $p_0' \cdots p_3'$ and $q_0' \cdots q_3'$.

Using the predicted values x_0', p_0', q_0' we calculate $f(x_0', p_0'), g(x_0', \mathrm{PO}', q_0'),$ and $h(p_0', q_0')$. Denote these values by f', g', h'.

The differences,

$$A = [(\Delta t)^2/2!]f' - x_2',$$
$$B = (\Delta t)g' - q_1',$$
$$C = (\mathrm{At})\, h' - p_1', \qquad \text{(A5)}$$

are then used to correct the predicted values in the following way:

$$x_n(t+\Delta t) = x_n' + f_{n2}A \qquad (n = 0, 1, \cdots, 5),$$
$$p_m(t+\Delta t) = p_m' + f_{m1}B \qquad (m = 0, 1, \cdots, 4), \qquad \text{(A6)}$$
$$q_m(t+\mathrm{At}) = q_m' + f_{m1}C\ t$$

where

$$f_{02} = 3/16, \quad f_{12} = 251/360, \quad f_{22} = 1,$$
$$f_{32} = 11/18, \quad f_{42} = 1/6, \quad f_{52} = 1/60, \qquad \text{(A7)}$$

and

$$f_{01} = 251/720, \quad f_{11} = 1, \quad f_{21} = 11/12,$$
$$f_{31} = 1/3, \quad f_{41} = 1/24. \qquad \text{(A8)}$$

It will be seen from Ref. 70 that these coefficients depend on the "order" of the procedure used. In our molecular dynamics runs on water we have used a fifth-order procedure for the center-of-mass motion and a fourth-order one for angular motion.

At the start of the calculation the most convenient procedure is to take all the derivatives equal to zero. In the case of interest here (Newton-Euler equations), the angular velocities (typified by q in the schematic presentation) can also be equated to zero at the start of the calculation. The "aging" of the run then necessarily leads to a solution effectively unrelated to the specific starting procedure.

APPENDIX B

In the convention utilized for the molecular dynamics calculations, each molecule experiences forces and torques due only to those other molecules within a cutoff radius R. In the presence of a uniform, weak, external electric field $\mathbf{E}_{ext}$, the system will develop a uniform polarization P. Classical electrostatics requires

$$4\pi\mathbf{P} = (\epsilon_0 - 1)\mathbf{E}, \qquad \text{(B1)}$$

where the electric field E is composed both of the imposed field $\mathbf{E}_{ext}$, and the internal field $\mathbf{E}_{int}$ due to the nonvanishing polarization

$$\mathbf{E} = \mathbf{E}_{ext} + \mathbf{E}_{int}. \qquad \text{(B2)}$$

The contribution of polarization in a small volume element δv at position r', to the internal field at position $\mathbf{r}$, is the following:

$$-\nabla_r[\delta v \mathbf{P}(\mathbf{r}')] \cdot \nabla_{r'}(|\mathrm{r}-\mathrm{r}'|^{-1}). \qquad \text{(B3)}$$

In writing an expression for the polarization P(r) for molecules at $\mathbf{r}$, that is consistent with the molecular dynamics, we clearly must integrate quantity (B3) only over the sphere of radius R surrounding position r:

$$4\pi\mathbf{P}(r) = (\epsilon_0 - 1)[\mathbf{E}_{ext} - \int_{|\mathbf{r}-\mathbf{r}'|\le R} d\mathbf{r}' \nabla_r \mathbf{P}(\mathbf{r}') \cdot \nabla_{r'}(|\mathbf{r}-\mathbf{r}'|^{-1})]. \qquad \text{(B4)}$$

The integral may easily be evaluated to yield:

$$4\pi\mathbf{P} = (\epsilon_0 - 1)[\mathbf{E}_{ext} - (4\pi/3)\mathbf{P}], \qquad \text{(B5)}$$

or

$$\mathbf{P} = [3(\epsilon_0 - 1)/4\pi(\epsilon_0 + 2)]\mathbf{E}_{ext}. \qquad \text{(B6)}$$

Not surprisingly, relation (B6) is exactly the same one that applies to the polarization of a spherical dielectric sample with a real boundary surface, placed in a vacuum region initially containing $\mathbf{E}_{ext}$ only. We may therefore call upon the Kirkwood theory of polar dielectrics,[30] which applies to those spherical specimen conditions.

Irrespective of boundary conditions, the polarization consists of a part $\mathbf{P}_\alpha$ due to induced molecular moments, plus a part due to reorientations that is proportional to $\langle M^2 \rangle$, the mean-square system moment in the absence of external fields[71]:

$$\mathbf{P} = \mathbf{P}_\alpha + (\mathrm{P}/3V)\langle M^2 \rangle \mathbf{E}_{ext}, \qquad \text{(B7)}$$

where V stands for the system volume. The import of expressions (B6) and (B7) taken together is that for a given ϵ_0, the quantity $\langle M^2 \rangle / V$ should be the same for the molecular dynamics situation as it is for a spherical dielectric sample in a vacuum.

Kirkwood[72] has shown that the local moment $\mathbf{m}$ of a fixed molecule and its immediate surroundings, in a dielectric sphere, is related to the average moment M of that sphere by

$$\mathbf{M} = [9\epsilon_0/(\epsilon_0 + 2)(2\epsilon_0 + 1)]\mathbf{m}. \qquad \text{(B8)}$$

It is precisely the distinction between these two moments which G_K and g_K for the dielectric sphere reflects, so we must have

$$G_K = [9\epsilon_0/(\epsilon_0 + 2)(2\epsilon_0 + 1)]g_K. \qquad \text{(B9)}$$

In view of the equivalence of the dielectric sphere to

the molecular dynamics system, the same relation applies to G_K and g_K for the latter, as shown by Eq. (4.17).

One should not take these considerations to mean that when $\mathbf{E}_{ext}$ vanishes, the polarization density surrounding fixed molecules in the two types of systems is the same (even if R for the molecular dynamics equals the dielectric sphere radius).

* Part of the work carried out at the Argonne National Laboratory was supported by the U.S. Atomic Energy Commission.

[1] A good review of the current situation is provided by D. Eisenberg and W. Kauzmann, *The Structure and Properties of Water* (Oxford U. P., New York, 1969).
[2] K. Morokuma and L. Pederson, J. Chem. Phys. **48**, 3275 (1968).
[3] P. A. Kollman and L. C. Allen, J. Chem. Phys. **51**, 3286 (1969).
[4] K. Morokuma and J. R. Winick, J. Chem. Phys. **52**, 1301 (1970).
[5] G. H. F. Diercksen, Chem. Phys. Letters **4**, 373 (1969).
[6] J. Del Bene and J. A. Pople, Chem. Phys. Letters **4**, 426 (1969).
[7] D. Hankins, J. W. Moskowitz, and F. H. Stillinger, Chem. Phys. Letters **4**, 527 (1970).
[8] J. Del Bene and J. A. Pople, J. Chem. Phys. **52**, 4858 (1970).
[9] D. Hankins, J. W. Moskowitz, and F. H. Stillinger, J. Chem. Phys. **53**, 4544 (1970).
[10] N. Metropolis, A. W. Rosenbluth, M. N. Rosenbluth, A. H. Teller, and E. Teller, J. Chem. Phys. **21**, 1087 (1953).
[11] B. J. Alder and T. E. Wainwright, J. Chem. Phys. **33**, 1439 (1960).
[12] S. W. Peterson and H. A. Levy, Acta Cryst. **10**, 70 (1957).
[13] J. D. Bernal and R. H. Fowler, J. Chem. Phys. **1**, 515 (1933).
[14] L. Pauling, J. Am. Chem. Soc. **57**, 2680 (1935).
[15] If interaction of the molecules with a container wall had to be explicitly considered, we would include single-molecule terms $V^{(1)}(\mathbf{x}_i)$ in this development. These extra potentials are unnecessary in the present context, however.
[16] F. H. Stillinger, J. Phys. Chem. **74**, 3677 (1970).
[17] A. Ben-Naim and F. H. Stillinger, "Aspects of the Statistical-Mechanical Theory of Water," in *Structure and Transport Processes in Water and Aqueous Solutions*, edited by R. A. Horne (Wiley–Interscience, New York, to be published).
[18] J. Corner, Trans. Faraday Soc. **44**, 914 (1948).
[19] The nuclear positions specified here do not conform exactly to the stable geometry of isolated water molecules. In particular, our O–H bonds are slightly too long (1 Å vs 0.957 Å measured length), and the bond angle somewhat too large (109° 28′ for the perfect tetrahedron vs 104° 31′ measured). However, there is experimental evidence that water molecule interactions in condensed phases may increase the average bond length (Peterson and Levy, Ref. 12) and theoretical evidence that they increase the average bond angle (Hankins, Moskowitz, and Stillinger, Ref. 9).
[20] H. Goldstein, *Classical Mechanics* (Addison-Wesley, Cambridge, Mass., 1953), p. 158.
[21] Reference 20, p. 134.
[22] A. Rahman, Phys. Rev. **136**, A405 (1964).
[23] It would be possible to restore energy conservation by forcing the cutoff to arise from a rapid decline in $S(r_{ij})$ from 1 to 0 when r_{ij} was close to 3.25σ. But this would entail unphysically large forces and torques at that large separation, which we consider to be undesirable.
[24] Some additional test runs were performed at the Bell Telephone Laboratories, Murray Hill, N.J., using a GE 635 computer.
[25] F. H. Stillinger and A. Ben-Naim, J. Phys. Chem. **73**, 900 (1969).
[26] H. S. Frank and W. Y. Wen, Discussions Faraday Soc. **24**, 133 (1957).
[27] G. Némethy and H. A. Scheraga, J. Chem. Phys. **36**, 3382 (1962).
[28] A. H. Narten and H. A. Levy, Science **165**, 447 (1969).
[29] A. H. Narten, ONRL Report No. ONRL-4578, July 1970. We are indebted to Dr. Narten for providing us with the atomic scattering factors used in the x-ray data treatment, whose original sources are identified in Ref. 29 of his report.
[30] J. G. Kirkwood, J. Chem. Phys. **7**, 911 (1939).
[31] The full pair correlation function $g^{(2)}(\mathbf{x}_1, \mathbf{x}_2)$ is normalized so as to approach $(8\pi^2)^{-1}$ at large separation r_{12}. In Eqs. (4.15) and (4.16), $\rho = \rho_0$ is the molecular number density.
[32] C. A. Coulson and D. Eisenberg, Proc. Roy. Soc. (London) **A291**, 444 (1966).
[33] L. Onsager and M. Dupuis, in *Electrolytes*, edited by B. Pesce (Pergamon, New York, 1962), p. 27.
[34] F. E. Harris, E. W. Haycock, and B. J. Alder, J. Chem. Phys. **21**, 1943 (1953); see also F. E. Harris and B. J. Alder, *ibid.* **21**, 1031 (1953).
[35] The members of the pair could simultaneously act either as proton donors to the third or as proton acceptors from the third.
[36] Realist Stereo Viewer, Realist, Inc., Menomonee, Wis.
[37] J. D. Worley and I. M. Klotz, J. Chem. Phys. **45**, 2868 (1966).
[38] G. E. Walrafen, J. Chem. Phys. **48**, 244 (1968).
[39] G. E. Walrafen, in *Hydrogen-Bonded Solvent Systems*, edited by A. K. Covington and P. Jones (Taylor and Francis, London, 1968), pp. 9–29.
[40] L. Pauling, *The Nature of the Chemical Bond* (Cornell U. P., Ithaca, N.Y., 1960), 3rd ed., p. 473.
[41] M. D. Danford and H. A. Levy, J. Am. Chem. Soc. **84**, 3965 (1962).
[42] O. Ya. Samoilov, *Structure of Aqueous Electrolyte Solutions and the Hydration of Ions* (Consultants Bureau, New York, 1965).
[43] These convex cages are illustrated by the clathrates in idealized form. Only by rotating its hydrogen bonds into eclipsed configurations can a cavity of sufficient size be built to accommodate the solute molecules.
[44] Reference 1, p. 89.
[45] R. Hausser, G. Maier, and F. Noack, Z. Naturforsch. **21a**, 1410 (1966).
[46] J. S. Murday and R. M. Cotts, J. Chem. Phys. **53**, 4724 (1970).
[47] The numerical calculation assumed that the autocorrelation function vanished beyond the "cutoff."
[48] J. G. Powles, J. Chem. Phys. **21**, 633 (1953).
[49] T.-W. Nee and R. W. Zwanzig, J. Chem. Phys. **52**, 6353 (1970).
[50] Reference 1, p. 207.
[51] S. G. Brush, Rev. Mod. Phys. **33**, 79 (1961).
[52] N. Bloembergen, E. M. Purcell, and R. V. Pound, Phys. Rev. **73**, 679 (1948).
[53] K. Krynicki, Physica **32**, 167 (1966).
[54] K. S. Cole and R. H. Cole, J. Chem. Phys. **9**, 341 (1941).
[55] E. H. Grant, T. J. Buchanan, and H. F. Cook, J. Chem. Phys. **26**, 156 (1957).
[56] L. Van Hove, Phys. Rev. **95**, 249 (1954).
[57] These Gaussian approximations are reviewed by A. Sjölander, in *Thermal Neutron Scattering*, edited by P. Egelstaff (Academic, New York, 1965), Chap. 7.
[58] It is however always Gaussian in both the short and long time limits.
[59] B. N. Brockhouse, Phys. Rev. Letters **2**, 287 (1959).
[60] D. J. Hughes, H. Palevsky, W. Kley, and E. Tunkelo, Phys. Rev. **119**, 872 (1960).
[61] K. S. Singwi and A. Sjölander, Phys. Rev. **119**, 863 (1960).
[62] C. T. Chudley and R. J. Elliott, Proc. Phys. Soc. (London) **77**, 353 (1961).
[63] M. Sakamoto, B. N. Brockhouse, R. G. Johnson, and N. K. Pope, J. Phys. Soc. Japan Suppl. B **17**, 370 (1962).
[64] Reference 1, p. 221.
[65] We are indebted to Dr. K. Gillen and Dr. D. C. Douglass for providing this value prior to publication.
[66] W. Kauzmann, Advan. Protein Chem. **14**, 1 (1959).
[67] G. Némethy, Angew. Chem. **6**, 195 (1967).
[68] J. A. Barker and R. O. Watts, Chem. Phys. Letters **3**, 144 (1969).
[69] J. S. Rowlinson, Trans. Faraday Soc. **47**, 120 (1951).
[70] C. W. Gear, ANL Report No. ANL-7126, 1966.
[71] F. E. Harris and B. J. Alder, Ref. 34.
[72] Reference 30, Eq. (12).